

**I Research Laboratory**

on. DC 20375-5000



**1-A244 041**



NRL Memorandum Report 6830



**On the Possibility of High Power Gyrotrons  
for Super Range Resolution Radar  
and Atmospheric Sensing**

WALLACE M. MANHEIMER

*Senior Scientist Fundamental Plasma Processes  
Plasma Physics Division*

December 20, 1991

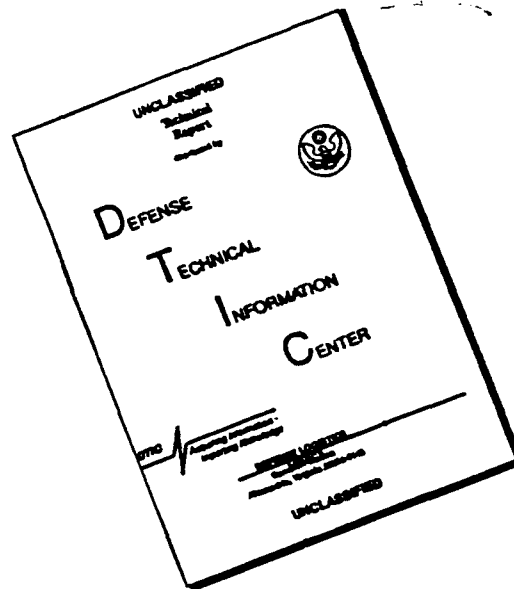
**DTIC  
ELECTE  
JAN 7, 1992  
S B D**

**92-00343**

Approved for public release; distribution unlimited.

REPORT DOCUMENTATION PAGE			Form Approved OMB No 0704-0188	
Public reporting burden for this collection of information is estimated to average 1 hour per response, including the time for reviewing instructions, searching existing data sources, gathering and maintaining the data needed, and completing and reviewing the collection of information. Send comments regarding this burden estimate or any other aspect of this collection of information, including suggestions for reducing this burden, to Washington Headquarters Services, Directorate for Information Operations and Reports, 1215 Jefferson Davis Highway, Suite 1204, Arlington, VA 22202-4302, and to the Office of Management and Budget, Paperwork Reduction Project (0704-0188), Washington, DC 20503.				
1. AGENCY USE ONLY (Leave blank)	2. REPORT DATE 1991 December 20	3. REPORT TYPE AND DATES COVERED NRL Memo Report 6830-Pre-assigned Number		
4. TITLE AND SUBTITLE On the Possibility of High Power Gyrotrons for Super Range Resolution Radar and Atmospheric Sensing		5. FUNDING NUMBERS 47-3637-0-1 91		
6. AUTHOR(S) Wallace M. Manheimer				
7. PERFORMING ORGANIZATION NAME(S) AND ADDRESS(ES) Naval Research Laboratory Code 4707 4555 Overlook Avenue, S.W. Washington, DC 20375-5000		8. PERFORMING ORGANIZATION REPORT NUMBER NRL Memorandum Report 6830		
9. SPONSORING / MONITORING AGENCY NAME(S) AND ADDRESS(ES) ONR Arlington, VA 22217-5000		10. SPONSORING / MONITORING AGENCY REPORT NUMBER		
11. SUPPLEMENTARY NOTES				
12a. DISTRIBUTION / AVAILABILITY STATEMENT Approved for public release; distribution unlimited.		12b. DISTRIBUTION CODE		
13. ABSTRACT (Maximum 200 words) High power gyrotrons have been developed recently; this makes a number of high power millimeter wave oscillators available. Currently their main application is the heating of fusion plasmas. This examines other potential applications for these rf sources. If used in multipulse radar mode, the pulses may be somewhat different from each other and this must be considered. A variant of coherent on receive can be used. With this, the entire pulse, not only the phase, is renormalized to a reference pulse. The data are analyzed off line. Possible applications of the quasi-optical gyrotron in a radar mode include exploiting its wide tuning range to achieve super range resolution and also remotely sensing the distribution of the size of ice crystals in cirrus clouds. Possible applications of a fixed frequency (94 GHz) gyrotron in radar mode include studying the structure of clouds. In a forward scatter mode, these high power sources could provide the capability to remotely sense the structure of clear air turbulence. The tunability of the quasi-optical gyrotron could also be exploited to rapidly perform measurements of relative humidity on the ground and in clouds, and to perform two-way earth to space measurements of upper atmosphere trace element concentrations.				
14. SUBJECT TERMS Gyrotron, Quasi-Optical Gyrotron, radar, remote sensing, atmospheric sensing		15. NUMBER OF PAGES 45		16. PRICE CODE
17. SECURITY CLASSIFICATION OF REPORT UNCLASSIFIED	18. SECURITY CLASSIFICATION OF THIS PAGE UNCLASSIFIED	19. SECURITY CLASSIFICATION OF ABSTRACT UNCLASSIFIED	20. LIMITATION OF ABSTRACT Unlimited	

# DISCLAIMER NOTICE



**THIS DOCUMENT IS BEST QUALITY AVAILABLE. THE COPY FURNISHED TO DTIC CONTAINED A SIGNIFICANT NUMBER OF PAGES WHICH DO NOT REPRODUCE LEGIBLY.**

## CONTENTS

1.	INTRODUCTION AND REVIEW OF NRL GYROTRONS AT ABOUT 100 GHZ .....	1
	A. The NRL 94 GHz Gyrotron .....	1
	B. The NRL Quasi-Optical Gyrotron .....	1
	C. Applications .....	3
2.	THE QUASI-OPTICAL GYROTRON FOR A HIGH-POWER, ULTRA WIDE BAND RADAR .....	5
	A. Radar Range Equation .....	5
	B. Single Pulse Radar Return .....	5
	C. Data Processing for Time Limited/Band Limited Functions .....	8
	D. High Range Resolution .....	9
	E. Rapid Range Imaging of Isolated Targets .....	11
3.	REMOTE SENSING OF CLOUDS AND ATMOSPHERIC PARTICULATE DISPERSION .....	12
	A. Radar Scatter from Clouds .....	12
	B. Analysis of Radar Returns from Clouds .....	13
	C. High Power Radar Echoes from Clouds .....	15
4.	REMOTE SENSING OF ATMOSPHERIC TURBULENCE .....	17
5.	REMOTE SENSING OF HUMIDITY .....	20
	A. Horizontal Path Average Humidity Measurement .....	20
	B. The Humidity Profile of Clouds .....	21
6.	REMOTE SENSING OF TRACE IMPURITIES IN THE UPPER ATMOSPHERE .....	22
	A. Trace Element Determination by Radiometry .....	22
	B. Ozone Detection by Backscatter from an Existing Satellite .....	24
	C. Measurement of Trace Impurity Density with a Specially Designed Satellite .....	25
	ACKNOWLEDGMENT .....	27
	REFERENCES .....	28

<b>Accession For</b>	
NTIS GRA&I	<input checked="" type="checkbox"/>
DTIC TAB	<input type="checkbox"/>
Unannounced	<input type="checkbox"/>
Justification	
By	
Distribution/	
<b>Availability Codes</b>	
<b>Dist</b>	<b>Avail and/or Special</b>
A-1	

# ON THE POSSIBILITY OF HIGH POWER GYROTRONS FOR SUPER RANGE RESOLUTION RADAR AND ATMOSPHERIC SENSING

## 1. Introduction and Review of NRL Gyrotrons at About 100 GHz

High power gyrotrons have been developed over the last 15 years in the United States<sup>1-5</sup>, the Soviet Union<sup>6,7</sup>, Europe<sup>8,9</sup>, Japan<sup>10</sup>, and China<sup>11</sup>. The research has principally been directed towards developing sources for electron cyclotron heating of fusion plasmas. The emphasis is on developing cw sources with high power. Commercial gyrotrons are available from Varian Associates, Palo Alto, Cal, with 300 kW at 28 GHz, 200 kW at 60 GHz, and 100 kW at 140 GHz. Varian is now working with a whispering gallery mode gyrotron, originally demonstrated at MIT, to develop a 1 MW gyrotron at 140 GHz<sup>12</sup>. At the Naval Research Laboratory, a 94 GHz gyrotron has been developed at 150 kW<sup>13,14</sup>, and the quasi-optical gyrotron has demonstrated 600 kW of peak power and tunability from about 80-130 GHz<sup>15-21</sup>. This power and tunability is a very new capability, and we are looking for additional applications. We examine here several possible applications involving high range resolution radar and atmospheric sensing. Since the sources we discuss are oscillators rather than amplifiers, all of the applications depend on a variant of coherent on receive data processing in radar systems. Specifically the entire amplitude and phase modulation of the transmitted and received waveforms are recorded digitally and then, processed, most likely off line. The ability to do this results from the extremely rapid advances in data processing technology. For instance a 500 MHz-1 GHz A to D converter, which is now state of the art, did not exist a few years ago. Similarly, if data processing capabilities increase at the same rate in the future, a few years from now real time data processing could be utilized for these applications. Section 2 will discuss in some detail the data processing techniques.

### A. The NRL 94 GHz Gyrotron

The 94 GHz gyrotron is a TE<sub>13</sub> mode gyrotron which has generated 150 kW of power in a 1 μs pulse at an efficiency of 15-20%. With appropriate cooling on the collector and window, it could operate at an average power of 10 kW. This is in fact only 10% of the average power Varian has demonstrated in their 140 GHz gyrotron. A mode convertor has been developed by General Atomics, San Diego, Cal, and is currently in place on our gyrotron. Conversion to the TE<sub>11</sub> mode has been demonstrated. Figure 1 is a photograph of the gyrotron laboratory. The equipment is compact and can easily be transported on a small truck. This capability to radiate average powers of order 10 KW at 94 GHz into the atmosphere represents a

very new capability. By contrast, the highest source available now is the Lincoln Laboratory Kwajalein radar tube which has a peak power of 6 KW and an average power of about 600 Watts and a bandwidth of about 1 GHz<sup>22</sup>.

### B. The NRL Quasi-Optical Gyrotron

The quasi-optical gyrotron is a very different sort of a gyrotron in an optical resonator. It has been developed at both NRL and Lausanne<sup>23,24</sup>. The beam propagation and the magnetic field are both transverse to the axis of the resonator. The mode output is taken by diffraction around the mirror. The diffraction is characterized by a fractional loss  $\nu$  per round trip of the radiation. Typically our experiment runs with  $\nu$ 's between 1 and 5%. Competition between different longitudinal modes is an important factor in the operation of the device. If the mirrors are very close together the mode density is low and it oscillates in only one mode at a time. However if the mirrors are further apart, it typically oscillates in several distinct longitudinal modes. Figure 2 is a photograph of the quasi-optical gyrotron. It is about as portable as the conventional gyrotron.

At NRL, two separate sets of experiments on the configuration with wide mirror separation have been conducted; one used a Varian VUW 8010 electron gun that can run up to about 75 kV and 20 Amps, and another used a Varian VUW 8144 electron gun which can operate up to about 100 kV and 60 Amps. Figure 3 is a plot of output power and efficiency for the latter gun, as a function of current, at a center frequency of about 120 GHz. The power peaks at 600 kW and the efficiency peaks at 12%.

One of the most attractive features of the quasi-optical gyrotron is its tunability. As the frequency changes, the only thing that changes in the cavity is the output coupling, which slowly decreases as a function of frequency. The quasi-optical gyrotron can be tuned in three ways: • The magnetic field can be varied over a fairly wide range. The power is relatively insensitive to field. Figure 4 shows a plot of mode frequency and power as a function of magnetic field for the lower power electron gun. The device can tune over about half an octave from about 80 to 130 GHz. • The device can be tuned with the beam voltage. Since the frequency scales as  $B/\gamma$ , the frequency can be raised by lowering the voltage. Figure 5 shows the Voltage tuning curve for the low power gun experiment.

input power is proportional to it. • The cavity can be tuned by adjusting the mirror separation, which can be done without breaking vacuum.

It is also possible that the quasi-optical gyrotron could operate at the second harmonic, although at lower power. An experiment can be designed with the harmonic having a lower starting current by exploiting the fact that the radiation beam has lower output coupling<sup>25,26</sup>. The Lausanne experiment has already seen evidence of harmonic operation<sup>24</sup>. If the quasi-optical gyrotron can run with harmonic operation, it opens the possibility of a single source covering the entire spectral region from 80 to 260 GHz. This would provide about 1 kW of average power in fundamental mode operation and about 10-100 Watts of average power in harmonic operation.

### C. Applications

With this review of the characteristics of the NRL gyrotrons, we continue with a discussion of potential applications for fielded systems. In any outdoor millimeter wave system, the question of interaction of the millimeter waves with the atmosphere is a crucial question. The propagation of millimeter wave power in the air has been studied extensively by Liebe,<sup>27</sup> and we use his model. Figure 6, provided by Liebe, shows the results of his model for attenuation and phase shift at sea level at 25°C as a function of frequency and relative humidity. Also a very useful information source is the *Near Millimeter Wave Technology Base Study*, edited by Kulpa and Brown<sup>28</sup>.

Possible applications for wideband, high-power millimeter waves include very wide band radar operation and atmospheric sensing. There is now interest in ultra wideband radars for fielded systems<sup>29,30</sup>. These ultra wideband systems are proposed with bandwidths from 1-3 GHz. However the quasi-optical gyrotron, in its fundamental mode operation has already demonstrated more than 40 GHz of tunability. Section 2 shows how this tunability can translate to bandwidth, giving 2-3 mm range resolution.

Section 3 discusses the possibility of using millimeter wave gyrotrons to obtain radar images of clouds. Since clouds are made from aerosols whose diameter is much less than a wavelength, the scattering is in the Rayleigh regime. The cross section scales as  $\lambda^{-4}$ ,

scattering is in the Rayleigh regime. The cross section scales as  $\lambda^{-4}$ , giving tremendous potential advantage to short wavelength systems. These systems are restricted principally by the unavailability of high power sources. In fact a series of radar images of clouds has been obtained by Lhermitte<sup>31-34</sup> by using an extended interaction oscillator at 94 GHz with an average power of 4 W. We discuss how the use of rf sources with much higher average power and tunability can greatly extend this capability by using standard meteorological data processing schemes<sup>35,36</sup> but applied to oscillators.

Section 4 discusses the use of high-power millimeter-wave sources to remotely sense the characteristics of clear air turbulent flow. At longer wavelengths, radar backscatter from clear air turbulence is routinely used to measure average wind velocity<sup>37-40</sup>. However very high power and very large antenna size are necessary and these measurements are almost always done from fixed sites. (Or else the experiments are done at very short range.) For instance the antenna in Ref. 39 was 26 m in diameter and the wavelength was about a foot. The peak power was about 4 MW. Thus the scattering was from fairly long wavelength components of the turbulent spectrum. The availability of high power millimeter wave sources opens up the possibility of scattering from much shorter wavelength fluctuations with a moveable facility. Specifically we investigate the way the minimum scale length of the turbulent flow, which is directly correlated with the turbulent dissipation, can be detected.

Section 5 discusses the remote measurement of humidity by two techniques. The first is a line of sight propagation measurement<sup>41</sup>, but now over a long horizontal path. The second measures humidity profile in clouds by comparing radar scatter at two frequencies. Section 6 examines the analogous application of the tunability of the quasi-optical gyrotron to the measurement of trace impurities in the upper atmosphere by two way propagation measurements (ie reflection from an orbiting satellite).

## 2. The Quasi-Optical Gyrotron for a High-Power, Ultra Wide Band Radar

In this section we show how an oscillator based radar can achieve a range resolution equal to  $c/2\Delta f$ . In the quasi-optical gyrotron, by stepping through a sequence of modes,  $\Delta f$  can be made equal to 40 GHz, the full tuning range. The key to oscillator use is in the data processing in the receiver. The transmitted and received pulse are each digitally recorded and an effective matched filter is generated numerically.

### A. Radar Range Equation

The power and wavelength of current gyrotrons make the radar resolution of very small targets possible at very large range. The radar equation for the range  $R$  is

$$R^4 \exp 2\alpha R = \lambda^2 G^2 P_t \sigma / (4\pi)^3 P_r.$$

where  $\alpha$  is the atmospheric attenuation,  $\lambda$  is the wavelength,  $G$  is the antenna gain,  $P_t$  is the transmitted power,  $\sigma$  is the target cross section, and  $P_r$  is the received power. The antenna gain is related to wavelength and diameter  $d$  of an ideal radiator by  $G = \pi^2 d^2 / \lambda^2$ . We assume that for reasonable radar performance the received power is 100 times the noise power,  $P_n = kT\Delta f$ , where  $\Delta f$  is the receiver bandwidth and the temperature is assumed to be 300°K. We consider two possibilities for the bandwidth. We first assume that the bandwidth is the width of the individual line of the quasi-optical gyrotron,  $\omega/Q$ , about 15 meters if  $Q = 10^4$ . In the second case, we consider the bandwidth to be pulse-limited; that is for a 10  $\mu$ s pulse the bandwidth is  $10^5$ , so range resolution in an individual pulse is 15 km. There is a wide frequency window, from about 70-110 GHz where the atmospheric attenuation in clear weather is less than 0.5 dB/km at relative humidity below 50%. Then if a one meter dish is used as the antenna and the transmit power is 300 kW, the maximum range of a 0.1  $\text{cm}^2$  target is 15 km for the wide band case and is 30 km for the narrow band case.

### B. Single Pulse Radar Return

For a target and transmitter that are both stationary, there is no frequency shift upon reflection. Therefore since the transmitted signal is square integrable in time from minus infinity to plus infinity, it can be written as a Fourier transform,

$$E_t(t) = \int df G_t(f) \exp 2\pi ift \equiv e_t(t) \cos[2\pi f_0 t + \phi_t(t)]. \quad (1)$$

Here  $f_0$  is assumed to be the carrier frequency and  $e$  and  $\phi$  are assumed to vary very slowly in time compared with  $f_0$ . We adopt a notation using  $E$  as a dependent variable in the time domain and  $G$  as a dependent variable in the frequency domain. We assume then that  $e$  and  $\phi$  can be digitized and computer analyzed. The digitizing does not have to be nearly fast enough to resolve  $f_0$ . We discuss later just what the requirements on the digitizer must be.

The fundamental assumption that we make here is that a return signal can be associated with one and only one transmitted pulse. Particularly, there does not appear to be any way that a radar based on an oscillator signal can separate returns from different range regions. Thus for a pulse separation  $\tau_p$ , returns from signals at distance greater than  $c\tau_p/2$  cannot be processed correctly. We now consider the returned signal associated with a particular transmitted signal.

The returned signal can be written as

$$\begin{aligned} E_r(t) &= \int df G_r(f) \exp 2\pi ift \equiv \int df s(f) G_t(f) \exp 2\pi ift \quad (2) \\ &\equiv e_r(t) \cos [2\pi f_0 t + \phi_r(t)] = \sum_j s_j e_t(t_j) \cos [2\pi f_0 t_j + \phi_t(t_j)], \end{aligned}$$

where  $s$  is the coefficient relating the transmitted to returned signal at frequency  $f$ . Here  $s = \lambda G \sqrt{\sigma} \exp(-\alpha R) / (4\pi)^{3/2} R^2$ . In the last line of Eq.(2), we assume that the returned signal is a summation over discrete scatterers at range  $R_j$ . The quantity  $t_j$  is  $t - 2R_j/c$ .

The key to using an oscillator rather than an amplifier then is to digitally record  $E_t(t)$ , or equivalently  $e_t(t)$  and  $\phi_t(t)$ , on each pulse and calculate  $G_t(f)$  by taking a Fourier transform. That is a very fast operation on a computer using fast Fourier transform routines. Then the same thing can be done on the returned signal to get  $G_r(f)$ . This then allows  $s$  to be calculated as a function of frequency as

$$s(f) = G_r(f)/G_t(f). \quad (3)$$

In practice, the transmitted signal does not have a meaningful reciprocal outside its bandwidth. Thus the usable bandwidth for an oscillator based system is less than the total bandwidth of the transmitted signal.

From the assumption that the system is stationary in time, we can calculate the radar return had the transmitted pulse been a desired pulse. Using a subscript d to denote the desired pulse on either the transmitted or returned pulse, we find

$$G_{rd}(f) = s(f) G_{td}(f). \quad (4)$$

The desired pulse has known properties, which we specify. Typically the desired pulse is a Gaussian with linear frequency chirp.

To get  $e(t)$  and  $\phi(t)$ , we send the signal and two reference signals, proportional to  $\sin$  and  $\cos$  of  $2\pi f_0 t$  through a mixer followed by a low pass filter. This will give two signals proportional to  $e(t)\sin\phi(t)$  and  $e(t)\cos\phi(t)$ , from which  $e$  and  $\phi$  can be obtained. They both vary very slowly in time compared with  $f_0$  and can be sampled and digitized. For instance, a 500 MHz A/D convertor with 8 bit digitizer is now state of the art. It will let the signal be digitized at this rate and allow 256 values of the function on a linear or logarithmic scale.

Of course the digitized samples must be processed by a discrete Fourier transform (DFT). To illustrate the nature of the range resolution obtained, the discrete calculations are approximated by continuous signals. Now let us Fourier transform the continuous transmitted signal. It is

$$G_t(f) = \int dt e_t(t) \cos[2\pi f_0 t + \phi_t(t)] \exp(-2\pi i f t). \quad (5)$$

Assuming that the fastest variation is from  $f_0$  and that we are looking at  $f > 0$  (the assumption is always that  $f_0 > 0$ ), we find that

$$G_t(f) = 0.5 \int dt e_t(t) \exp [2\pi i \delta f t + i \phi_t(t)], \quad f > 0 \quad (6)$$

where  $\delta f = f_0 - f$ . Thus the Fourier transform can be calculated from only a knowledge of  $e$  and  $\phi$  and only by operating on a time scale much slower than  $f_0$ , that is a time scale on which the data can be digitized. From a calculation of both  $G_t(f)$  and  $G_r(f)$ , the cross section  $s(f)$  can be calculated. From this we can calculate  $G_{rd}(f)$  from the knowledge  $G_{td}(f)$ .

The next step is calculating of  $e_{rd}(t)$  and  $\phi_{rd}(t)$ . From the definition of the Fourier transform, we find with a simple calculation that

$$e_{rd}(t) \exp i \phi_{rd}(t) = \int_0^\infty df G_{rd}(f) \exp (-2\pi i \delta f t). \quad (7)$$

Thus  $e_{rd}(t)$  and  $\phi_{rd}(t)$  can be obtained from the returned signal entirely by considering the slow time scale and without digitizing anything at frequency  $f_0$ .

Once we have the e's and  $\phi$ 's for the desired transmitted and returned signals, we form the matched filter response for the  $n^{\text{th}}$  range bin,

$$M_n = \int dt e_{td}(t-t_n) e_{rd}(t) \exp i[\phi_{rd}(t) - \phi_{td}(t-t_n)] \equiv \sum_i \int dt s_i e_{td}(t-t_n) e_{td}(t_i) \exp i[\phi_{td}(t_i) - \phi_{td}(t-t_n) - 4\pi f_0 R_i/c]. \quad (8)$$

Note that with this sort of signal processing, there is no single matched filter for the radar; rather, a separate matched filter is generated numerically for each radar pulse. This filter response then characterizes the cross section of the range interval centered at  $t=t_n$  or  $R_n = ct_n/2$ . If we assume that the desired transmitted signal is a Gaussian envelope,  $e_{td}(t) = e_0 \exp-(t/T)^2$ , with a linear frequency chirp,  $\phi_{td} = 0.5\alpha t^2$ , the integrals can be done for both the matched filter response and for the Fourier transforms. The results are

$$G_t(f) = \{\sqrt{\pi} e_0 T / [1 - i\alpha T^2/2]^{1/2}\} \exp[-\pi^2 \delta f^2 (T^{-2} + i\alpha) / \{T^{-4} + \alpha^2/4\}] \quad (9)$$

and

$$M_n = (\sqrt{\pi}/2) e_0^2 T \sum_i s_i \exp(-4\pi i f_0 R_i/c) \times \exp\{-(t_n - 2R_i/c)^2 [1/2T^2 + \alpha^2 T^2/8]\}. \quad (10)$$

The range resolution is determined by the fall off of the Gaussian. If this is dominated by the frequency chirp, the range resolution goes roughly as  $c\alpha T/\sqrt{8} \approx c/\Delta f$  where  $\Delta f$  is the frequency spread of the transmitted pulse.

### C. Data Processing for Time Limited/ Band Limited Functions

Although a function that is limited in both time and band is not possible, it is a useful approximation and idealization and gives important insight into the needs of the data processing system. The Gaussian waveform with the linear chirp is a reasonable approximation to a time-limited, band-limited function, and other functions may be better still. The transmitted pulse is assumed to be limited to time between 0 and  $T_t$ . The

received pulse is then limited to times between  $2R_{\min}/c$  and  $T_t+2R_{\max}/c$ , where  $R_{\min}$  and  $R_{\max}$  are the minimum and maximum range. Depending on the spatial extent of the target, the time of the returned pulse can be comparable to or much longer than the transmitted pulse. Note that if the returned signal is much longer than the transmitted signal, more spectral density is needed to resolve it in the Fourier domain. However the maximum bandwidth required is determined by the transmitted signal.

Since the incident and returned signals are limited in time to a time we call  $T_0$ , we can regard these signals as periodic with period  $T_0$  as long as we are careful to always stay within the time  $0 < t < T_0$ . Thus the signal can be regarded as a discrete Fourier summation

$$f(t) = \sum_n g(n) \exp 2\pi i n t / T_0, \quad 0 < t < T_0. \quad (11)$$

If the signal is band-limited as well as time-limited, then  $g(n)$  is non zero only for  $|n| < N$ . Then  $f(t)$  is needed only at  $2N$  discrete, equally spaced values of  $t$  to solve for the  $2N$  values of  $f(n)$ . Thus the waveforms must be sampled twice per period at the maximum frequency, and this gives *all* the information there is to be had about the function.

#### D. High Range Resolution

Now let us consider using the full bandwidth of the NRL quasi-optical gyrotron in a stepped frequency mode to achieve very high range resolution of an isolated, stationary target. Let us consider the target to be near the center of a range cell for a single pulse. Then, according to Eq.(11),

$$M(q) = (\sqrt{\pi}/2)e_0^2 T \sum_i s_i \exp (-4\pi i f_q R_i / c), \quad (12)$$

where now we use an index  $q$  for the mode frequency ( $f_q = qc/2L \equiv qw$ ) to denote that it will change from pulse to pulse and we have deleted the index  $n$  on  $M$  because everything is assumed to take place in a single range cell, that is, at a single value of  $n$ . Here  $f_q$  is the frequency of the local oscillator, which is nearly equal to the frequency of the quasi-optical gyrotron when it operates in the desired mode. Also we will use a dimensionless range to the target  $\rho_i = 2wR_i/c$ . As the quasi-optical gyrotron shifts from one mode to another,  $q$  will increase from a minimum value  $q_1$  up to a maximum value  $q_2$ .

Note that the reference frequency  $f_q$  must be determined very accurately because any error in  $4\pi f_q R/c$  must be significantly less than one from pulse to pulse. Thus as one goes from frequency to frequency, the local oscillator frequency must be known very accurately (but not necessarily the high-power oscillator frequency). Fortunately such sources have been developed. For instance the Hughes Series 4774xH phase locked Gunn oscillator seems to have sufficient stability. The phase is locked to a high harmonic of a low frequency source (tens of megahertz) and the Hughes catalog shows that phase noise is down 60db compared to the main signal 10 Hz away from the carrier frequency, and the amplitude noise is even lower.

For now, assume that all ranges  $\rho_i$  are known and form the summation

$$\begin{aligned} \sum_{q_1}^{q_2} M(q) \exp 2\pi i \rho_j q &= (\sqrt{\pi}/2) e_0^2 T \sum_i \sum_{q_1}^{q_2} s_i \exp -2\pi i q (\rho_i - \rho_j) \\ &= \sum_i s_i [\exp -\pi i (\rho_i - \rho_j) (q_2 - q_1)] \{ \sin \pi (\rho_i - \rho_j) (q_2 + 1 - q_1) / \sin \pi (\rho_i - \rho_j) \}. \end{aligned} \quad (13)$$

The last line in Eq.(14) comes from summing up the geometric series in  $q$ . The term in the brackets is very much like a delta function and maximizes at  $\rho_i = \rho_j$ . Thus, regarding the left hand side of Eq.(14), which is a function of  $\rho_j$ , we see that contributions to it come only from nearby targets. The contribution to the left hand side of Eq.(14) then comes from targets within the first maximum of the sin function in the brackets, or  $R_j - R_i < c/2(f_2 - f_1)$ , where we have gone back to dimensional units. This is the conventional for range resolution a radar of having frequency spread  $f_2 - f_1$ .

Let us now approximate the target as a series of discrete scatterers at ranges given by  $\rho_p = p/(q_2 + 1 - q_1)$ , where  $p$  is an integer that ranges from a minimum value of  $p_1$  to a maximum value of  $p_2$ . Then the brackets on the right hand side of Eq.(14) becomes proportional to a Kronecker delta and (changing the indices of summation from  $ij$  to  $pp'$ ) we find

$$\sum_{q_1}^{q_2} M(q) \exp 2\pi i p q / (q_2 + 1 - q_1) = (q_2 + 1 - q_1) (p_2 + 1 - p_1) \sigma_p. \quad (14)$$

Thus if the targets are assumed to be discrete points, separated by the range resolution and localized at a grid in range that is reciprocal to the grid of discrete frequencies, the cross section at each position is simply the discrete Fourier transform of the filter response as a function of  $q$ . The maximum

number of elements that can be resolved is then  $q_2 - q_1 + 1$  as long as  $p_2 - p_1 = q_2 - q_1$ .

Notice however that if  $p$  increases by  $q_2 + 1 - q_1$ , the left hand side of Eq.(14) is unchanged. Thus there is an ambiguity if the spatial extent of the target is larger than  $L$ , which is the mirror separation in the quasi-optical gyrotron. This ambiguity can be mitigated by varying the mirror separation.

Figure 7 is a block diagram of the circuitry, for the case of operation in one mode at a time. Notice that after the A/D converter, the blocks do not correspond to physical circuit components, but to elements or subroutines of a computer code.

### E. Rapid Range Imaging of Isolated Targets

We have seen how the quasi-optical gyrotron can be used for obtaining range resolution for isolated targets with roughly 2-3 mm range resolution. However one drawback is that the target must be stationary, and the time to perform the image is determined by the time it would take the quasi-optical gyrotron to tune through its entire tuning range. This is a period of several minutes as the experiment is set up now. Several approaches are possible to achieve much faster tuning.

One approach to rapid range resolution using the full bandwidth of the device would be a high voltage quasi-optical gyrotron. This would be able to tune through a much large range by changing the voltage, which can be done very quickly. However this experiment is only in the concept stage at this time. Another approach is to use a trim coil inside the superconducting coil of the quasi-optical gyrotron to electronically sweep the magnetic field. The case of a 5 kG trim field oscillating at 0.5 Hz, appears to be fairly straightforward; the case of a 5 kG field oscillating at 5 Hz appears to be possible but difficult<sup>42</sup>. Half of the period of oscillation then defines the minimum time in which the range image can be formed.

### 3. Remote Sensing of Clouds and Atmospheric Particulate Dispersion

In this section we discuss the use of the gyrotrons and quasi-optical gyrotrons for remote sensing of clouds or particulates in the atmosphere. The properties of many of the different types of clouds are summarized in Ref 28.

#### A. Radar Scatter from Clouds

Since the droplet diameter in the cloud is much less than a quarter of the wavelength, the scattering is in the Rayleigh regime and the cross section is given by

$$\sigma = \pi^5 |K^2| D^6 / \lambda^4. \quad (15)$$

where  $D$  is the aerosol diameter,  $\lambda$  is the wavelength, and  $K = (m^2 - 1)/(m^2 + 2)$  and  $m$  is the index of refraction. For water at millimeter wavelength,  $|K^2|$  is given by about 0.8. The strong increase of cross section with inverse wavelength is a potential advantage of a millimeter wave system. So is the fact that a tightly focused beam can be produced with a relatively small antenna. Since the radar beam intersects the entire cloud, the radar cross section is the cross section of each droplet times the number of droplets in the beam. The volume of the cloud examined is the area of the radar beam times the range resolution distance, denoted  $h$ . For cloud studies, the radar reflectance  $\eta$  is the usual parameter used, where  $\eta = \sum_i \sigma_i G / 4\pi R^2 h$ , the cross section per unit volume, where the summation is over the droplets in the volume. For a typical cloud, like those studied by Lhermitte, the droplet diameter is about  $10\mu\text{m}$  and the droplet density is about  $100\text{cm}^{-3}$ , so the reflectivity is about  $3 \times 10^{-12} \text{cm}^{-1}$ . With such small reflectances and low power of the transmitter, the observation of the cloud is difficult. For Lhermitte's case, with a range of 3 km, a transmitted power of 1 kW, a range resolution distance  $h$  of  $6 \times 10^3 \text{cm}$ , and an effective aperture of  $4 \times 10^3 \text{cm}^2$ , the received power is about  $10^{-13} \text{W}$ . Lhermitte's receiver had a noise of about  $5 \times 10^{-13}$  so his signal power is below the noise power, and he had to integrate the signal over a considerable number of pulses to get good data. In his case, he runs the EIO at about 10 kHz pulse repetition rate and integrates for 3 s, or about  $3 \times 10^4$  pulses. He finds that the meteorological conditions remain reasonably constant for these 3s.

Lhermitte used an oscillator, not an amplifier as his microwave source. To do the coherent signal integration and Doppler processing, he uses a coherent on receive approach and corrects the phase of the received signal according to the phase of the transmitted signal. Except for the random phase from pulse to pulse, the EIO has extremely good signal properties. In fact, this was the reason for Lhermitte's choice of an EIO over a magnetron, which could operate at somewhat higher average power.

## B. Analysis of Radar Returns from Clouds

Here we briefly examine the use of a gyrotron oscillator as a source for radar studies of clouds using the principles sketched out in Section 2. Thus, as in the last section, we build the data processing scheme around the matched filter response, which also optimizes signal to noise ratio.

The cloud consists of a number of individual scatterers denoted by the index  $i$ . Each scatterer moves with velocity  $v + \delta v_i$ , where  $v$  is the average velocity in the range cell and  $\delta v_i$  is a random velocity whose average value is zero. Each velocity is sufficiently small that the scatterers can be regarded as stationary during the individual radar pulse. However the velocities will be Doppler resolved by looking at reflections from a long sequence of pulses. The return signal from the desired pulse can be constructed as in the previous section. In this case it is

$$e_{rd}(t) \exp i \phi_{rd}(t) = \sum_i s_i e_{dt}(t - 2R_i/c) \exp i \phi_{td}(t - 2R_i/c) \\ \times \exp i [-(4\pi f_0/c)(R_i + vt + \delta v_i t)] + N_d(t), \quad (16)$$

where where the summation is over droplets and  $N_d(t)$  is the noise signal operated on by the same operations that turn the received signal into the received signal from the desired waveform. All conditions regarding the usable portions of the spectrum discussed in the previous section still apply.

We assume that the radar transmits  $P$  pulses spaced by a time  $\tau$ , and calculate the matched filter response for each pulse for each range cell. Henceforth we will neglect the noise to simplify the analysis. We assume that  $P$  is large enough that the signal, which is proportional to  $P^2$  is sufficiently larger than the noise, which is

proportional to P. Furthermore, the high power sources we are considering should be less constrained by noise than was the case for Lhermitte. If the desired pulse is Gaussian with linear frequency chirp, the matched filter response is also a Gaussian centered about the center of the range cell. We will make the simplifying assumption that the matched filter response is

$$M_{np} = (\sqrt{\pi/2})e_0^2 T \sum_i s_i \exp[-(4\pi i f_0/c)(R_i + (v + \delta v_i)p\tau)] \quad (17)$$

where the index n denotes the range cell and p the pulse. That is we assumed each droplet is at the center of the range cell and the summation is over the droplets in the range cell. Associated with the index p is the Fourier transform variable  $2\pi z/P$  where z takes on integer values from zero to P-1. Then one can define

$$Q_n(z) = \sum_p M_{np} \exp 2\pi i p z/P \quad (18)$$

To obtain the reflectance, one forms the summation  $\sum_z |Q_n(z)|^2 \equiv Q_n$ . In addition to the summation over z, there are four other summations over i and p and over the analogous variables j and q in the complex conjugate. The summation over z is a simple summation of a geometric series and turns out to be equal to P if p=q and zero otherwise. We then separate the summation over i and j into a sum of two summations, one having i=j and one having i≠j. The former is a simple summation over reflectances over the individual droplets and has N terms in it where N is the number of droplets. The latter is the sum of 0.5N(N-1) terms, each one having essentially a random phase. The rms value of a summation of N<sup>2</sup> random phases is about N, so for each value of p, the summation over the i's and j's will have about the same order of magnitude. However the summation over the p index greatly reduces the value of the i≠j summation. In this summation, the sum over p is also a geometric sum which can be done simply. The result is that this summation is very small unless  $\delta v_i - \delta v_j < c/4f_0 P\tau$ . Thus if the velocity spread of the droplets is sufficiently large, the i≠j sum is small compared to the i=j sum. If f<sub>0</sub> is 94 GHz, and Pτ = 0.1 sec, the spread of droplet velocities only has to be large compared to 1 cm/s, a condition almost certainly satisfied for droplets in clouds. Thus we find that

$$Q_n = \{0.8P^2\pi^7 e_0^4 T^2 d^4 \exp(-2\alpha R_n)/16\lambda^6 R_n^4\} \sum_i D_i^6 \quad (19)$$

where we have used the relation between  $s$  and  $\sigma$  for the droplets, the expression for cross section in Eq.(15), and the fact that the antenna gain is  $\pi^2 d^2 / \lambda^2$ , where  $d$  is the antenna diameter.

To determine the average velocity of the droplets, one forms the summation  $\sum_z z |Q_n(z)|^2 \equiv F_n$ . An analogous calculation gives the result

$$F_n = [2P f_0 v_n \tau / c] \times Q_n \quad (20)$$

where we have explicitly denoted the dependence of velocity on range cell. Other moments of the distribution of velocities can be found by taking other moments of  $Q_n$ . Equations (19) and (20) show how the reflectance and relative velocity in a range cell are calculated from the backscattered radar signal. Figure 8 is a schematic of the circuitry for the Doppler cloud radar.

### C. High Power Radar Echoes from Clouds

With this introduction to the radar echoes from clouds or particulates, let us examine the cloud measurements Lhermitte has made and see how they can be enhanced with the use of a high power or tunable transmitter. One of the first measurements was the reflection from a thunderstorm in the Miami, Florida area. The range at which he was able to operate was about 20-30 km. However since the air at ground level was quite humid, he was only able to observe the tops of the clouds. For instance one of his observations is at an angle of  $34^\circ$  and a range of 20 km, so that he observes an altitude of 11 km. He points out that at a  $30^\circ$  elevation, the two way absorption was 12 dB, whereas at a  $7^\circ$  angle, it is 50dB. His transmitter however had an average power of only 4 W. A gyrotron transmitter, operating with an average power of 4 kW would be able to examine the same cloud at much lower elevation.

One of the easiest types of clouds to observe with a 94 GHz radar is high altitude cirrus clouds. Reference 31 points out that these clouds can be observed with a radar even when they cannot be seen visually. The reason is that a small number of large size ice crystals are in the cloud. Lhermitte points out that such a cloud with a single 2 mm ice crystal per cubic meter has about 35 dB more reflectivity than a fair weather cloud with the same water content. The tunability of the quasi-optical gyrotron could then aid in

remotely sensing the distribution of ice crystal sizes in such clouds. As long as the ice crystal diameter is less than about a quarter of a wavelength, the scattering is in the Rayleigh regime. Other than the  $\lambda^{-4}$  dependence of the scattered power on the wavelength, there is no information concerning the distribution of sizes. However for larger crystals, there are resonances due to Mie scattering. Figure 9 shows the backscattering cross section of water and ice spheres at 94 GHz as a function of diameter (taken from Ref. 31). The quasi-optical gyrotron, especially if it could operate at both the cyclotron frequency and its harmonic, could irradiate the cloud at several frequencies between about 80 and 260 GHz; the radiation could be spread out over several Mie resonances, depending on the size of the crystals. The backscatter cross section as a function of frequency then gives information regarding the distribution of scatterer size. While the size distribution cannot be exactly inverted from the scattered spectrum, information can be obtained as in microwave propagation experiments through rain<sup>43</sup>.

The other observation Lhermitte made is of small fair weather cumulus clouds. A small cloud passes directly overhead at an altitude of about 1.5 km; as it goes by, the reflectivity and vertical velocities are measured by the radar at a series of range cells 65 m in depth. The cloud is overhead for about 2 minutes. Since each vertical scan takes 3 s, there are about 40 vertical scans in the cloud and about 6-8 range cells. A higher power transmitter could enhance these measurements in a number of ways. First, in doing the same measurement as Lhermitte at higher power, the radar beam could be scanned from side to side in the cloud so that a three dimensional image of the cloud could be formed. Second, the range cell could be reduced to perhaps 10 m (a 10 MHz bandwidth) so that the cloud could be examined vertically in much greater detail. Third, the higher power could be used for greater range to image clouds that are not directly overhead. This not only gives another view of the cloud, but it also gives another component of velocity. For clouds with a horizontal range of perhaps 10 km, the radar would give a Doppler velocity in a direction that is almost horizontal.

#### 4. Remote Sensing of Atmospheric Turbulence

Here we discuss the potential use of the quasi-optical gyrotron as a remote sensor for atmospheric turbulence. High power gyrotrons appear to provide a unique capability for sensing the inner scale length of the turbulence in an open atmosphere at fairly long range. This is an important property, because standard theories relate it closely to the strength of the turbulence. Before proceeding, we briefly review some properties of atmospheric turbulence, as summarized in Doviak and Zrnic<sup>37</sup>.

Power feeding the turbulence is provided at large scale length. Nonlinear convection of the fluid then generates shorter and shorter scale lengths until the very short scale motions are dissipated by viscosity. This intermediate range of cascade is called the inertial range. The energy per unit mass of the fluid per unit  $k$  is  $dE(k)/dk$  and has units  $m^3/s^2$ . The power per unit mass provided at small  $k$  is denoted  $\epsilon$ , and it has units  $m^2/s^3$ . For steady state turbulence,  $\epsilon$  is also the power dissipated per unit mass at large  $k$ , which is also equal to the power convected through the inertial range in  $k$  space. The convection velocity through  $k$  space,  $dk/dt$ , is related to  $E$  and  $\epsilon$  through the relation  $\epsilon = (dk/dt) \times (dE(k)/dk)$ . The assumption now is that  $E(k)$  depends only on  $k$  and  $\epsilon$ . Assuming a polynomial relation, there is only one which is dimensionally correct,

$$dE(k)/dk = A \epsilon^{2/3} k^{-5/3}, \quad (21)$$

where  $A$  is a dimensionless constant. Doviak and Zrnic use the value of  $\epsilon$  to characterize the turbulence, Table 1 gives their characterization. Generally, the spectrum seems to be borne out by experiment.

The minimum value of  $k$  is determined by the power input at large scale. The maximum value of  $k$  is determined by the viscous dissipation. The time for the power in this range of  $k$  to dissipate by viscosity is given by  $1/\nu k^2$ , where  $\nu$  is the kinematic viscosity in  $m^2/s$ . The time the spectral energy remains in a region of size  $k$  is given by  $k/(dk/dt)$ . Equating these two times, we find that  $k_{max}$  is proportional to  $\epsilon^{1/4}/\nu^{3/4}$ . Doviak and Zrnic give the proportionality of  $1/5$ , so

$$k_{max} = 0.2\epsilon^{1/4}/\nu^{3/4}. \quad (22)$$

At sea level,  $v \approx 10^{-5} \text{ m}^2/\text{s}$ , so for strong turbulence, the minimum distance,  $2\pi/k$  is about 1 cm.

Scattering from clear air turbulence is caused by fluctuations in the index of refraction which in turn is caused mostly by fluctuations in water vapor content. To determine the spectrum of index of refraction fluctuations, the spectrum of a scalar quantity passively advected by the turbulent field must be calculated.<sup>37,44,45</sup> The basic assumption of all workers, however, is that the passively advected scalar has the same spectrum as the energy, so  $|\ln(k)|^2 = C_n^2 k^{-5/3}$ , where  $C_n^2$  is in units of  $\text{m}^{-2/3}$ . Doviak and Zrnik's characterization the coefficient  $C_n^2$  in terms of the strength of the turbulence is shown in Table 1.

We now consider the scattering from the turbulence. Assuming that  $\delta n$  is small, the Born approximation for the case that the electric field is evaluated in the far field ( $k_0 D^2/r < 1$ , where  $D$  is the diameter of the scattering volume), gives the scattered electric field at the point  $r$  is given by

$$E_s = (k_0^2 E_i / 4\pi r) \exp i k_0 r \int d^3 r' \delta n(r') \exp i(k_i - k_s) \cdot r' \quad (23)$$

where  $E_i$  is the incident electric field in the scattering region,  $k_i$  is the incident, and  $k_s$  is the scattered wave vector. The integral is over the scattering volume, which is defined as the intersection of the patterns of the transmitting and receiving antennae. Assuming that the scattering volume is very large compared to the scale size of the index fluctuation, we find

$$|E_s|^2 = k_0^4 E_i^2 V C_n^2 |k_i - k_s|^{-11/3} / 8r^2 \quad (24)$$

where  $V$  is the scattering volume. In performing the integrals and manipulations, we have made use of the fact that the spectral density per unit  $k$  space volume is given by  $|\ln(k)|^2 / 4\pi k^2$  for a homogeneous, isotropic spectrum. Also, we have made use of the fact that the density of states in  $k$  space is  $V / (2\pi)^3$ . If the scattering angle is  $\theta$ , then  $|k_i - k_s| = 2k_i \sin \theta / 2$ .

For backscatter ( $\theta = \pi$ ) and  $k = 1800 \text{ m}^{-1}$  (94 GHz), the scattering wave vector is almost certainly larger than  $k_{\text{max}}$ , so there should be virtually no backscatter. However there will be scatter in other directions. The use of powerful gyrotrons at 94 GHz (and possibly at

35 GHz also) opens up the possibility of examining the inner scale length by oblique scattering measurements. The inner scale length could be inferred from the angle at which the scattering disappears. Frequency tunability, as available with the quasi-optical gyrotron could reduce the number of receiving antennae.

Let us consider a specific example to show how the availability of 94 GHz gyrotrons with over 100 kW of power can render possible a scattering measurement of the inner scale length. The scattering volume is then roughly  $LD^2$  where  $L$  is the length of the intersection of the two antenna patterns and we have assumed the incident beam is the more tightly focused of the two. Then we relate the field amplitude to the power density and add to Eq.(24) additional factors accounting for the atmospheric attenuation. Then Eq.(35) can be rewritten as

$$P_r = k_0^4 A_e L P_i C_n^2 |k_i - k_s|^{-11/3} \exp[-\alpha(r_i + r_s)] / 8r_s^2 \quad (25)$$

where  $P_r(t)$  is the incident (reflected) power,  $A_e$  is the aperture of the receiving antenna,  $\alpha$  is the atmospheric attenuation, and  $r_i$  is the range from the incident antenna to the scattering region. Let us choose a configuration in which the scattered radiation is in the far field. Although this is not absolutely necessary, it does simplify both the analysis and the interpretation of any data.

Take a transmitting antenna of  $D=3$  m which can focus radiation down to a spot 2 m, 2.5 km away, and a range to the receiver of 10 km. For relative humidity 50% or less, the attenuation is 10 db or less. For 94 GHz radiation with a 3 m receiving antenna and an assumed inner scale length of 3 cm ( $|k_i - k_s|=200$ ), we find that  $P_r/P_i \approx 2 \times 10^{-17}$ , assuming strong turbulence,  $C_n=3 \times 10^{-13}$ , and also  $L=D/\sin\theta$ . If the incident power is  $10^5$  W, the received power is about  $2 \times 10^{-12}$  W, 4 times the noise power at 300°K. Integration over a small number of pulses could further enhance SNR. Consider the alternative of using an EIO having a power of 1 kW and an average power of 4 W. Now the signal is a factor of 25 below the noise level, and this is for fairly strong turbulence. It is unlikely that the SNR could be significantly increased by integrating over a large number of pulses; at the shortest scale length (3 cm), the correlation time of the turbulence is undoubtedly very short ( $10^{-2}$ s at 3m/s), so the scattered pulses would not be coherent with one another for very long.

## 5. Remote Sensing of Humidity

In this section we briefly examine the possibility of using the high power and tunability of the quasi-optical gyrotron to remotely sense humidity in two ways. First we consider remote sensing on a long horizontal path, second we consider sensing the humidity profile of clouds by radar sensing in a DIAL mode.

### A. Horizontal Path Average Humidity Measurement

As pointed out in Ref. 28, many attenuation measurements have been made, both in the laboratory and in the field. These are difficult measurements due to the necessity of keeping the electronics sufficiently stable. Generally the experiments use cw sources chirp the frequency. The measurements we discuss here are basically single or multi-frequency measurements with pulses several microseconds long. The high power and short pulse length are advantageous because the conditions of the atmosphere will be constant for one series of measurements. The quasi-optical gyrotron provides a unique capability in that it can be tuned (with second harmonic operation) to the center of the absorption peak at 180 GHz, and it has enough power to propagate long distances in the atmosphere.

Operating the quasi-optical gyrotron at several modes near 180 GHz allows several frequencies within the absorption peak to be examined. Furthermore, not only absorption, but also phase shifts, which may be easier to calibrate, can be measured. By comparing with dispersive delay times  $\tau_d$ , also shown in Fig. 6, water concentration can be inferred. The phase shift  $\Delta\Phi$  is given in terms of the dispersive delay time by  $\Delta\Phi = 2\pi f\tau_d$ . If the receiver is at range  $R$  from the transmitter, and the transmitted pulse at frequency  $f_i$  (one of the modes of the oscillator) is given by  $E_i(t)\cos[2\pi f_i t + \phi_i(t)]$ , the received pulse will be given by

$$E_r = E_{ri}(t)\cos [2\pi f_i t + \phi_{ri}(t)] = E_i(t-R/c)\exp(-\alpha_i R)\cos[2\pi f_i t + \phi_{ri}(t)], \quad (26)$$

where  $\alpha_i$  is the attenuation and  $\phi_{ri}(t) = 2\pi f_i R/c + \phi_i(t-R/c) + \Delta\Phi_i$ . The  $E$ 's and  $\phi$ 's can be measured from the transmitted and received signal, as discussed in Section 2. Assuming that the range is not known accurately to a fraction of a wavelength, it can be eliminated between the various modes. Specifically, we find

$$f_j[\phi_{ri}(t) - \phi_i(t-R/c)] - f_i[\phi_{rj}(t) - \phi_j(t-R/c)] = f_j\Delta\Phi_i - f_i\Delta\Phi_j \quad (27)$$

so all phase shifts can be found in terms of a single reference shift. Thus from measurements of the phase and attenuation, the relative humidity can be inferred.

### B. The Humidity Profile of Clouds.

Another application is the remote sensing the humidity profile of clouds with the use of radar backscatter at two different frequencies. The droplets serve as the scatterers and the relative attenuation between the different range cells in the cloud can give information to the humidity profile in the cloud. As is apparent from Eq.(19), the reflectivity from a range cell in a cloud depends on the number of scatterers as well as the attenuation between the transmitter and the reflecting region of the cloud. Consider the return from the range cell in the cloud which is nearest the transmitter. At a single frequency, only the product of the scattering and the attenuation from the transmitter to the bottom of the cloud can be inferred. However by using two frequencies, the attenuation and the scattering can each be obtained as long as the attenuation is known as a function of frequency (as given in for instance Fig.6). In doing so, one must also account for the fact that the summation over droplets may have a frequency dependence due to the fact that the geometry of the scattering volume may also depend on frequency for a specified antenna. By stepping up in the cloud from one range cell to another, the humidity profile can be obtained within the cloud. The quasi optical gyrotron, which has the capability of both high power and tunability, could provide a unique source source for such a measurement by examining the cloud at first 90 and then 130 GHz.

## 6. Remote Sensing of Trace Impurities in the Upper Atmosphere

We now look into whether the tunability of the quasi-optical gyrotron can be used to detect trace elements other than water. At sea level, this appears to be an extremely difficult measurement due to the fact that the pressure broadening of the absorption lines is substantial (typically about 2-3 GHz), and the impurity concentration is very low. Distinguishing the impurity absorption from the water vapor absorption, which dominates it by many orders of magnitude, does not appear to be a simple task. However for impurities in the upper atmosphere, the pressure broadening is much less, as is the amount of water vapor to interfere with the measurement.

The idea is then to bounce the radiation at a frequency near the absorption line off an orbiting satellite, detect the backscattered radiation, and examine the absorption and phase shift as a function of frequency to determine the concentration of the impurity. (One might think that at high altitude, the molecule would spontaneously re-emit before it is collisionally deexcited, so that a satellite would not be necessary. However the time for spontaneous reemission for rotationally excited molecules varies from about  $10^4$  to  $10^9$  s, so this is not the case<sup>45</sup>.) Measurements like this are currently performed by radiometry, whereby the thermal spectrum of the atmosphere is measured and related to the trace elements. The scattering scheme we discuss here would appear to have several potential advantages over radiometry. First of all, the effect is doubled because two way propagation doubles the path length. Secondly, phase measurements as well as amplitude measurements now become possible. Finally because the power of the millimeter wave sources is large, the measurements give snapshots of the atmospheric concentration in very short times, milliseconds to seconds depending on the concentration and antenna size. This contrasts with the many hours or even days it takes to do an analogous measurement by ground based radiometry.

### A. Trace Element Determination by Radiometry

In radiometry, the thermal spectrum of millimeter wave radiation is detected and related to the concentration of the element.<sup>46</sup> These measurements can be absorption measurements, for instance measuring the absorption of sunlight at frequencies near the absorption line. Also the thermal emission can be studied, and this is what we concentrate on here. For the atmosphere which

radiates as a black body (if it were optically thick) the radiation temperature is related to the intensity of radiation by the Rayleigh-Jeans, or actually the Planck law. If the radiation is emitted from a region with temperature  $T$  and  $s$  is the path length, then the radiation temperature  $T_R$  at the receiving antenna is given by

$$T_R = \int_h^{\infty} T(s)\alpha(s)\exp(-\tau(s)), \quad \tau(s) = \int_h^s \alpha(s')ds' \quad (28)$$

where  $\alpha(s)$  is the sum of the absorption coefficient of all gases to be considered and  $\tau$  is the opacity. For a propagation medium which is optically thin, as is the case for millimeter waves in the upper atmosphere, the presence of the gas of interest gives rise to a slight increase in radiation temperature at the frequencies near the absorption line.

The upper atmosphere is typically at a temperature of between about 200-300°K. Thus for an optically thin propagation medium, the ratio of antenna temperature due to the impurity to the source temperature (that is the upper atmosphere) is roughly the opacity. For ozone at 110.8 GHz, in a standard atmosphere, the zenith opacity is about 6% and the antenna temperature is about 10° K at the line center.<sup>47</sup> If the line shape is Lorentzian, as is characteristic of a pressure broadened line, the temperature as a function of frequency reflects this line shape. The line width is a function of altitude. If sufficient resolution of temperature as a function of frequency is available, the profile of ozone density as a function of altitude can often be inverted.<sup>48</sup>

This temperature due to the impurity is generally small compared to the atmosphere temperature. In radiometry, the relative temperature fluctuation through a channel of bandwidth  $B$  is given by  $(BY)^{-1/2}$  where  $Y$  is the integration time, so small temperature changes due to an impurity can be resolved by long integration time. Parrish et al<sup>49</sup> have recently studied trace element concentrations in the upper atmosphere. These are all related to the ozone cycle, and as such, the altitudes are about 40 km, so the pressure broadening is about 10-20 MHz. They found that at 277 GHz, ozone had a temperature of 8°K and the integration time was an hour to achieve SNR of 600. They also found that ClO had a temperature about 0.06° at 279 GHz. To achieve SNR of 25 took 36 hours over 9 days. The weakest line they were able to detect was the 266 GHz line of H<sub>2</sub>O. This line had a temperature of about 0.015°K and took 55 hours to resolve the line.

## B. Ozone Detection by Backscatter from an Existing Satellite

We now consider the use of the quasi-optical gyrotron as a tunable source for active detection of ozone. We consider the 110.8 GHz absorption line; a frequency at which the quasi-optical gyrotron can easily be tuned. To provide a two way path, we exploit reflection from an existing satellite. There are many satellites and pieces of space debris whose low earth orbits are known to high precision. As we will see however, not all are suitable as reflectors; to be a viable reflector, the size of the satellite must be quite small.

In active probing of the upper atmosphere, both amplitude and phase are available to analyze. Here we consider only the phase, since the analysis of the amplitude is no different in principle from radiometry. For a Lorentzian line shape centered at  $\omega_0$ , the total complex attenuation and phase shift,  $\Xi$  for the two way propagation is given by

$$\Xi = \tau v \{ (v + i(\omega - \omega_0)) / (v^2 + (\omega - \omega_0)^2) \}, \quad (29)$$

where  $\tau$  is the two way opacity at the line center, and  $v$  is the pressure broadening. At the altitude in question,  $v/2\pi$  is about 10 MHz. Thus, for ozone, whose two way zenith opacity is 12%, and whose opacity at  $45^\circ$  is about 20%, the total phase shift as one crosses the line could be as high as  $10^\circ$ - $15^\circ$ . Analogous to Eq. (26), if the incident wave is at frequency  $f_i$  the phase of the returned signal is given by

$$\begin{aligned} \phi_{ri} = & 2\pi R(2f_i + \delta f_{di})/c + \phi_{ti}(t - 2R/c) + \Delta\Phi_i(f_i) \\ & + \Delta\Phi_i(f_i + \delta f_{di}) + \Phi + \delta\Phi(f_i, p) \end{aligned} \quad (30)$$

For a satellite of known orbit, the Doppler shift can be calculated very accurately, and can be as high as a few MHz for 100 GHz incident radiation. In Eq.(30),  $\Delta\Phi_i(f_i)$  is the ozone generated phase shift at frequency  $f_i$  on the way up,  $\Delta\Phi_i(f_i + \delta f_{di})$  is the ozone generated phase shift of the Doppler shifted wave on the way down,  $\Phi$  is the phase shift from all other components, determined from for instance a standard atmosphere model, and  $\delta\Phi(f_i, p)$  is the phase shift generated by the satellite, where  $p$  denotes pulse number. The satellite generated phase shift varies with frequency because different frequencies have different scattering centers; it varies with

p because the satellite might change its orientation, due to rotation, during the pulse train. The difficulty is that  $\delta\Phi(f_i, p)$  is basically unknown. One can only perform the measurement if  $\delta\Phi(f_i, p)$  is independent of both  $f_i$  and p.

The satellite will be considered to be a set of discrete scatterers, with index m, centered at R and having position  $\delta R_m$  from the center. It is the  $\delta R_m$ 's which contribute the essentially random nature of the phase. If the frequency difference between the waves in the spectrum is denoted  $\delta f$ , then the contribution to the phase shift is  $4\pi\delta R\delta f/c$ , where for convenience, we have deleted subscripts. As long as this is small compared to the phase shift we are attempting to measure, it can be neglected. This then puts a limit on both the size of the satellite and also on the frequency spread. For ozone at 40 km altitude, assume a width of 20 MHz. At a  $45^\circ$  inclination angle, the phase shift we are measuring is about 0.2 radians. This means that the satellite or debris radius must be small compared to about 30 cm. Also, the phase might change pulse to pulse because of the rotation of the satellite, so the total measurement time must be small compared to a rotation period of the satellite, typically tens of seconds. Thus, a small existing satellite or piece of space debris, which is not rotating violently, could serve as a reflector for rapid, ground based ozone measurement.

We now consider what it would take to do an ozone measurement at a transportable facility. If we consider the antenna to be 3 m (a gain of 70 dB), a bandwidth which is pulse time limited ( $10^5 \text{ s}^{-1}$ ), a transmitted power of 1 MW, a range of 300 km, a 5 cm radius spherical scatterer, and a receiver temperature of  $1000^\circ\text{K}$ , we find that SNR of  $10^3$ . This corresponds to a phase resolution in a single pulse of about  $(\text{SNR})^{-1/2}$ . If 20 pulses within a time of a tenth of a second to a second are transmitted within the 20 MHz interrogation bandwidth, the phase shift within the absorption line can be resolved and the ozone density can be inferred.

### C. Measurement of Trace Impurity Density with a Specially Designed Satellite

The satellite generated phase shift can be greatly reduced or eliminated by the use of a specially designed satellite. Specifically, we consider the use of a spherical satellite, whose cross section is independent of orientation, and whose cross section as a function of frequency can be accurately calculated and measured. For trace

elements such as ClO or HO<sub>2</sub>, discussed in Ref. 49 , the total phase shift across the absorption line is  $10^{-3}$ - $10^{-4}$  radians. Thus the satellite must be smooth to about this fraction of a wavelength. However since we are considering millimeter waves, this fraction of a wavelength means an optical quality reflector, a standard capability. We consider specifically a 20 cm radius spherical reflector. In one rocket launch, a number of these, perhaps ten or so, could be placed into orbit to provide nearly continual, permanent coverage.

We now consider reflection from one of these specially designed satellites to measure trace impurity density. For instance the 242 GHz ClO absorption<sup>50</sup> line would be observable with the quasi-optical gyrotron at the second harmonic. It has a limb temperature of few degrees Kelvin, and a ground temperature of about 0.05°K looking near the horizontal. Since an active measurement has double the path length, we assume that at an angle of 45° to the zenith, a value of about 0.03°K, or a phase shift of about  $3 \times 10^{-4}$  radians. The total two way absorption, from sea level, at 240 GHz, at an inclination of 45° to the zenith is less than 10 dB for relative humidity less than 50%. If a high altitude is chosen for the measurement, the absorption is less still. We consider first the use of a satellite tracking station, with an antenna diameter of 20 m. Consider a receiver temperature now of 100°K, a total atmospheric attenuation of 10 dB, and a radiated power, assumed to be 100 kW at the second harmonic. Then for a 10  $\mu$ s pulse, SNR is about  $2 \times 10^7$  . Ten pulses will then give sufficient SNR to accurately measure a phase shift  $3 \times 10^{-4}$  radians. This time is so short that it could even be possible to do the measurement over a longer time with a 3m dish in a portable facility. However the satellite would have to be accurately tracked over the measurement time. To conclude, the tunability of the quasi-optical gyrotron gives a capability to rapidly measure upper atmosphere ozone concentrations with existing equipment. With specially designed satellites and accurate satellite tracking, it could give rapid measurement of trace impurities at much lower concentration.

## Acknowledgment

The author thanks David Kerr of the NRL Radar Division and Donald Wehner of NOSC for a number of useful discussions concerning radar data analysis; as well as William Hooper and Philip Schwartz of NRL's Space Sensing Division for a number of discussions regarding remote sensing. Also he thanks H. Liebe for providing Fig 9. This work was supported by the Office of Naval Research.

## References

1. K. Felch, R. Bier, L. Fox, H. Huey, H. Jory, N. Lopez, J. Manca, J. Shively, and S. Spang, *Int. J. Electronics*, 57, 815, 1984
2. K. Felch, R. Bier, L. Craig, H. Huey, L. Ives, H. Jory, N. Lopez and S. Spang, *Int. J. Electronics*, 61, 701, 1986
3. K. Kreischer, J. Schutkeker, B. Danly, W. Mulligan, and R. Temkin, *Int. J. Electronics*, 57, 835, 1984
4. K. Kresicher and R. Temkin, *Phys. Rev. Lett.*, 59, 547, 1987
5. K. Kreischer, T. Grimm, W. Guss, A. Mobius, and R. Temkin, *Phys Fluids B2*, 640, 1990
6. A. Gaponov, V. Flyagin, A. Goldenberg, G. Nusinovich, S. Tsimring, V. Usov, and S. Vlasov, *Int. J. Electronics*, 51, 277, 1981
7. A. Fix, V. Flyagin, A. Goldenberg, V. Khizhnyak, S. Malygin, S. Tsimring, and V. Zapevallov, *Int. J. Electronics*, 57, 821, 1984
8. A. Bensimhon, G. Faillon, G. Garin, and G. Mourrier, *Int. J. Electronics*, 57, 805, 1984
9. E. Borie, G. Dammertz, O. Dumbrajs, G. Gantenbein, T. Geist, G. Hochschild, M. Kuntze, Z. Liao, A. Mobius, H. Nickel, B. Piosczyk, M. Thumm, and H. Wenzelburger, 15<sup>th</sup> IR and Millimeter Waves Conference, Temkin ed, SPIE Vol 1514, p493, 1990
10. Y. Mitsunaka, K. Hayashi, Y. Hirata, Y. Itoh, T. Kariya, M. Komuro, T. Okamoto, Y. Okazaki, T. Sugawara, A. Yano, T. Nagashima, and K. Sakamoto, 15<sup>th</sup> IR and Millimeter Waves Conference, Temkin, ed, SPIE Vol 1514, p318, 1990
11. H. Guo, D. Wu, G. Liu, Y. Maio, S. Qain, and W. Zin, *IEEE Trans. Plasma Sci.*, 18, 326, 1990
12. K. Felch, C. Hes, H. Huey, E. Jongewaard, H. Jory, J. Nielson, R. Pendleton, and M. Tsurulnikov, 15<sup>th</sup> IR and Millimeter Waves Conference, Temkin ed, SPIE Vol 1514, pp 315, 1990

13. G. Bergeron, M. Czarnaski, and M. Rhinewine, *Int. J. Electronics*, 69, 281, 1990
14. M Rhinewine, T. Hargreaves, M. Barsanti, G. Bergeron, and M. Czarnaski, 15<sup>th</sup> IR and Millimeter Waves Conference, Temkin ed, SPIE Vol 1514, pp 578, 1990
15. P. Sparangle, J. Vomvorides, and W. Manheimer, *Appl. Phys. Lett.*, 38, 310, 1981
16. A. Bondeson, W. Manheimer, and E. Ott, *Infrared and Millimeter Waves*, Ch 7, Vol 9, Academic Press, 1983
17. T. Hargreaves, K. Kim, J. McAdoo, S. Park, R. Seeley, and M. Read, *Int. J. Electronics*, 57, 977, 1984
18. A. W. Fliflet, T. Hargreaves, W. Manheimer, R. Fisher, M. Barsanti, B. Levush, and T. Antonsen, *Phys Fluids*, B2, 1046, 1990
19. A. Fliflet, T. Hargreaves, R. Fisher, W. Manheimer and P. Sprangle, *J. Fusion Energy*, 9, 31, 1990
20. A. Fliflet, T. Hargreaves, W. Manheimer, R. Fisher, and M. Barsanti, *IEEE Trans Plasma Sci*, 18, 306, 1990
21. T. Hargreaves, A. Fliflet, R. Fisher, M. Barsanti, W. Manheimer, B. Levush, and T. Antonsen, *Int. J. Electronics*, to be published
22. A. Reich and S. Hong, "High Power 35 and 94 GHz Instrumentation Radar" Lincoln Laboratory, Lexington, MA, June, 1984
23. T. Tran, 14<sup>th</sup> IR and Millimeter Waves Conference, SPIE Vol 1240, 1990
24. S. Alberti, M. Podrozzi, M. Tran, J. Hogge, T. Tran, P. Muggli, H. Jodicke, and H. Mathews, *Phys. Fluids*, B2, 2544, 1990
25. B. Levush, A. Bondeson, W. Manheimer, and E. Ott, *Int. J. Electronics*, 54, 749, 1983

26. B. Levush and W. Manheimer, *Intl. J. IR and Millimeter Waves*, 4, 877, 1983
27. H. Liebe, *International J. IR and Millimeter Waves*, 10, 631, 1989
28. *Near Millimeter Wave Technology Base Study*, Vol 1, S. Kulpa and E. Brown, Co-Chairmen HDL-SR-79-B, Available from U.S. Army Material Development and Readiness Command, Alexandria, VA, 22333
29. M. Skolnik, *An Introduction to Impulse Radar*, NRL Memorandum Report 6755, Nov, 1990
30. *Assessment of Ultra-Wideband (UWB) Technology*, C. Fowler, Chairman, *IEEE AES Magazine*, November, 1990
31. R. Lhermitte, *J. Atmospheric and Oceanic Tech.* 4, 36, 1987
32. R. Lhermitte, *IEEE Trans. Geoscience and Remote Sensing*, 26, 207, 1988
33. R. Lhermitte, *Geophysical Res. Lett.*, 14, 707, 1987
34. R. Lhermitte, *Geophysical Res. Lett.*, 15, 1125, 1988
35. *Doppler Radar and Weather Observations*, R. Doviak and D. Zrnica, Academic Press, 1984, Chapters 4-6
36. *Introduction to Radar Systems*, M. Skolnik, McGraw Hill, 1980, p 106
37. Doviak and Zrnica, Chapters 10 and 11
38. B. Balsley and K. Gage, *Bull. Am. Meteorological Soc.* 63, 1009, 1982
39. V. Peterson and B. Balsley, *Geophysical Res. Lett.* 6, 933, 1979
40. K. Gage and B. Balsley, *Bull. Am. Meteorological Soc.* 59, 1074, 1978

41. T. Manabe, R. DeBolt, and H. Liebe, 12<sup>th</sup> Intl Conf IR and Millimeter Waves, Orlando, Fla, 1987, Sponsored by IEEE MTT, IEEE Cat# 87CH2490-1
42. K. Efferson, American Magnetics Corporation, private communication, March, 1991
43. Furuhashi and Ihara, IEEE Trans Antennas and Propagation, AP-29, 275, 1981
44. R. J. Hill J. Fluid Mechanics, 88, 541, 1978
45. V.I. Tatarskii, *Effects of the Turbulent Atmosphere on Wave Propagation*, Available from US Dept Commerce, UDC 551.510, ISBN, 07065 0680 4 Natl. Tech. Inf. Service, Springfield, VA
46. R.M. Price, *Radiometer Fundamentals*, in *Methods of Experimental Physics 12B*, M. Meeks, ed, p 201, Academic Press, 1976
47. J. Waters, *Absorption and Emission by Atmospheric Gases*, in *Methods of Experimental Physics 12B*, M. Meeks ed, p 142, Academic Press, 1976
48. A. Randegger, Pure and Applied Geophys. 118, 1052, 1980
49. A. Parrish, R. deZafra, P. Soloman, and J. Barrett, Radio Science, 23, 106, 1988
50. S. Ochiai and H. Masuko, 15<sup>th</sup> IR and Millimeter Wave Conference, Temkin, ed, SPIE Vol 1514, 41, 1990

Table 1 — The Characterization of Turbulent Strength

Turbulence	$C_n^2 \text{ m}^{-2/3}$	$\epsilon \text{ m}^2/\text{s}^{-3}$
Weak	$6 \times 10^{-17}$	$3 \times 10^{-3}$
Moderate	$2 \times 10^{-15}$	$8.5 \times 10^{-3}$
Severe	$3 \times 10^{-13}$	$6.8 \times 10^{-2}$

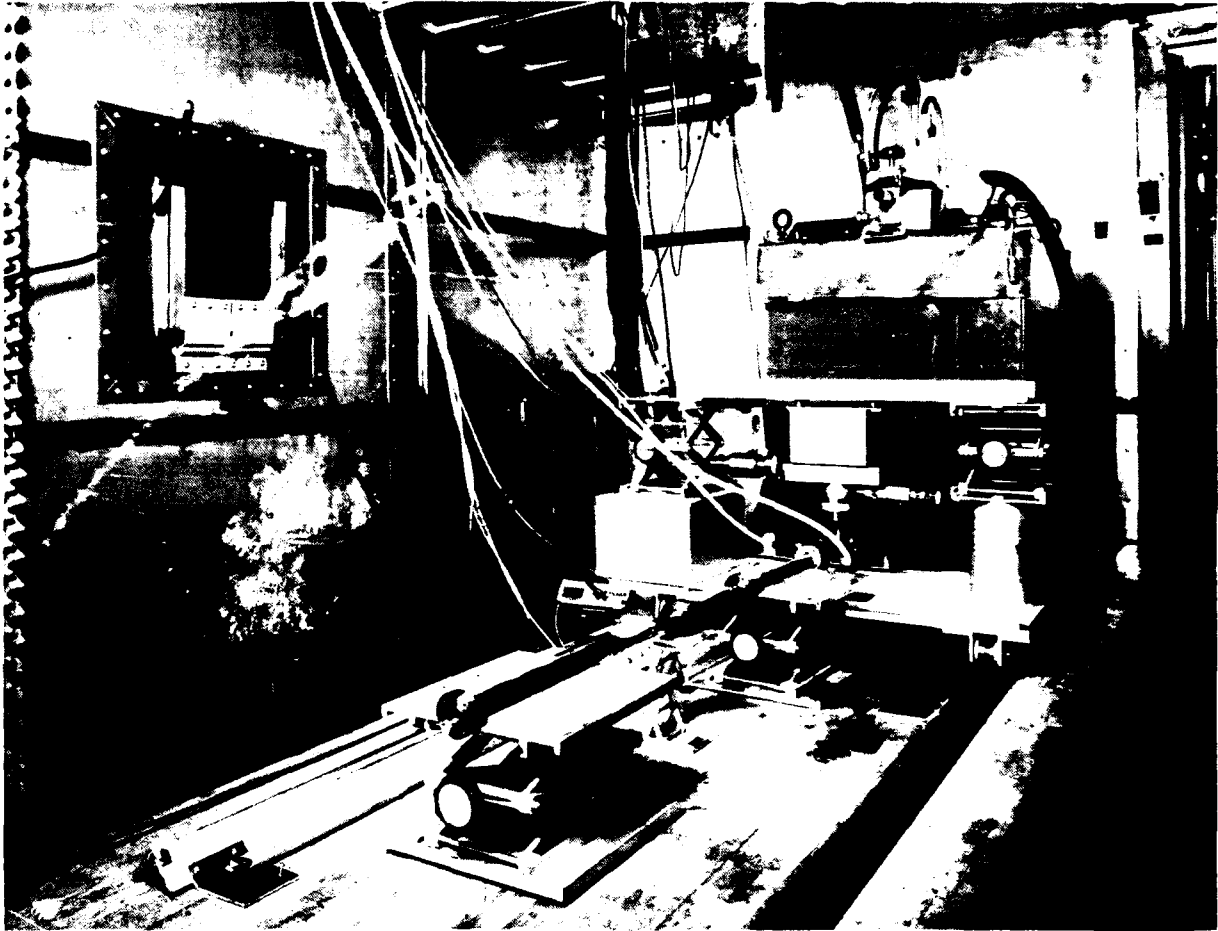


Fig. 1 — Photograph of the 94 GHz gyrotron with the mode converter in place

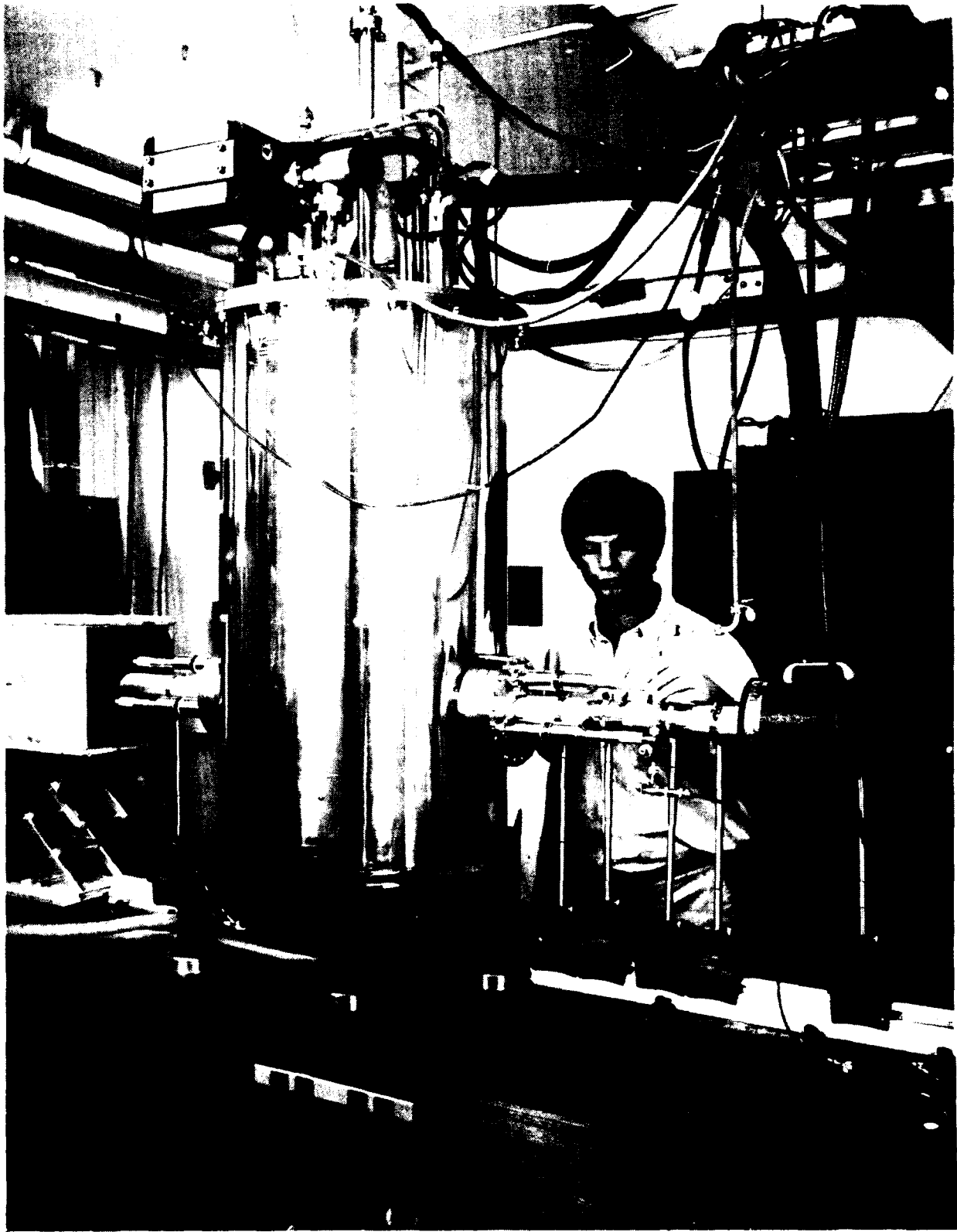


Fig. 2 — Photograph of the quasi-optical gyrotron

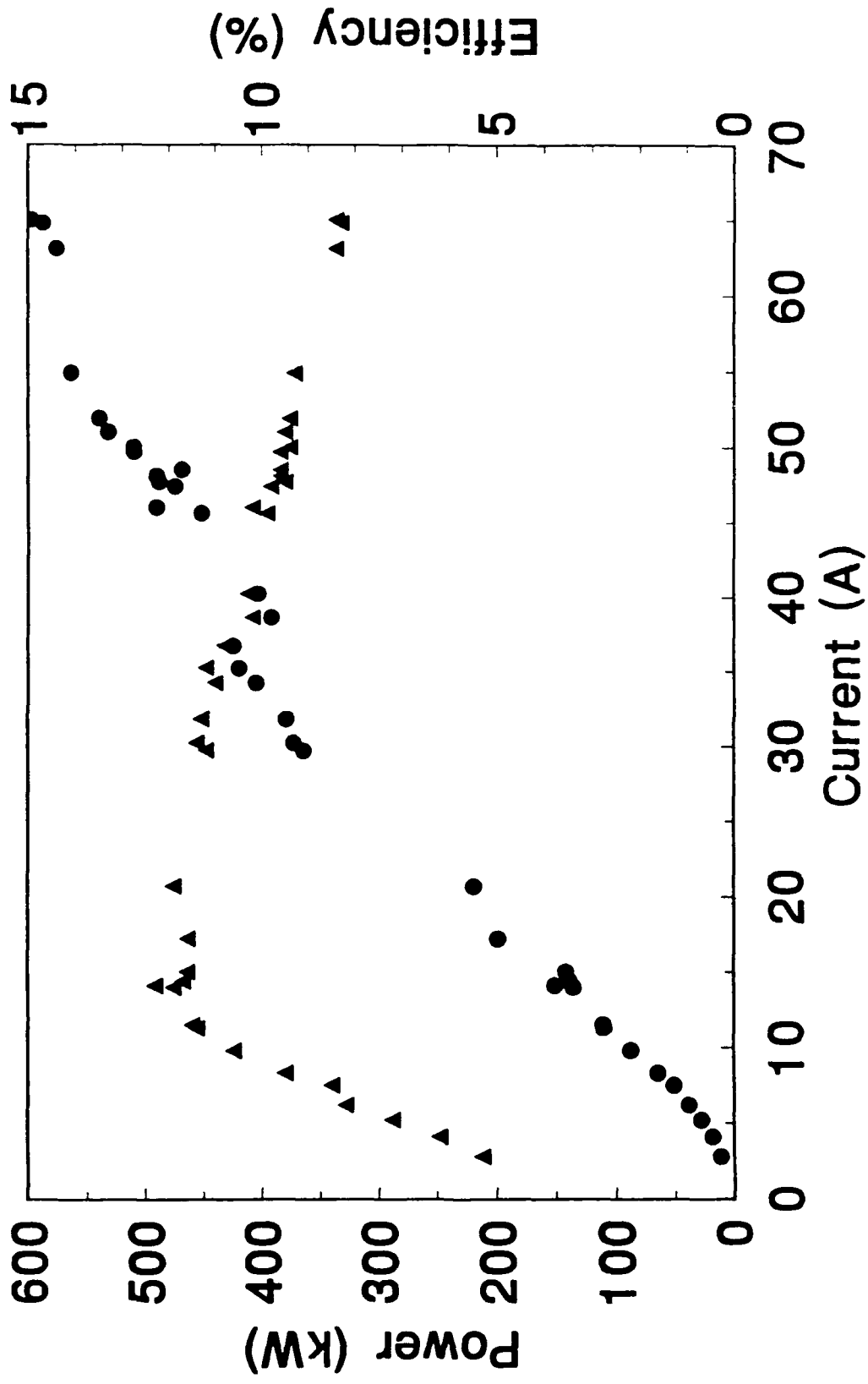


Fig. 3 — Power (circles) and efficiency (triangles) of the quasi-optical gyrotron as a function of current at about 120 GHz.

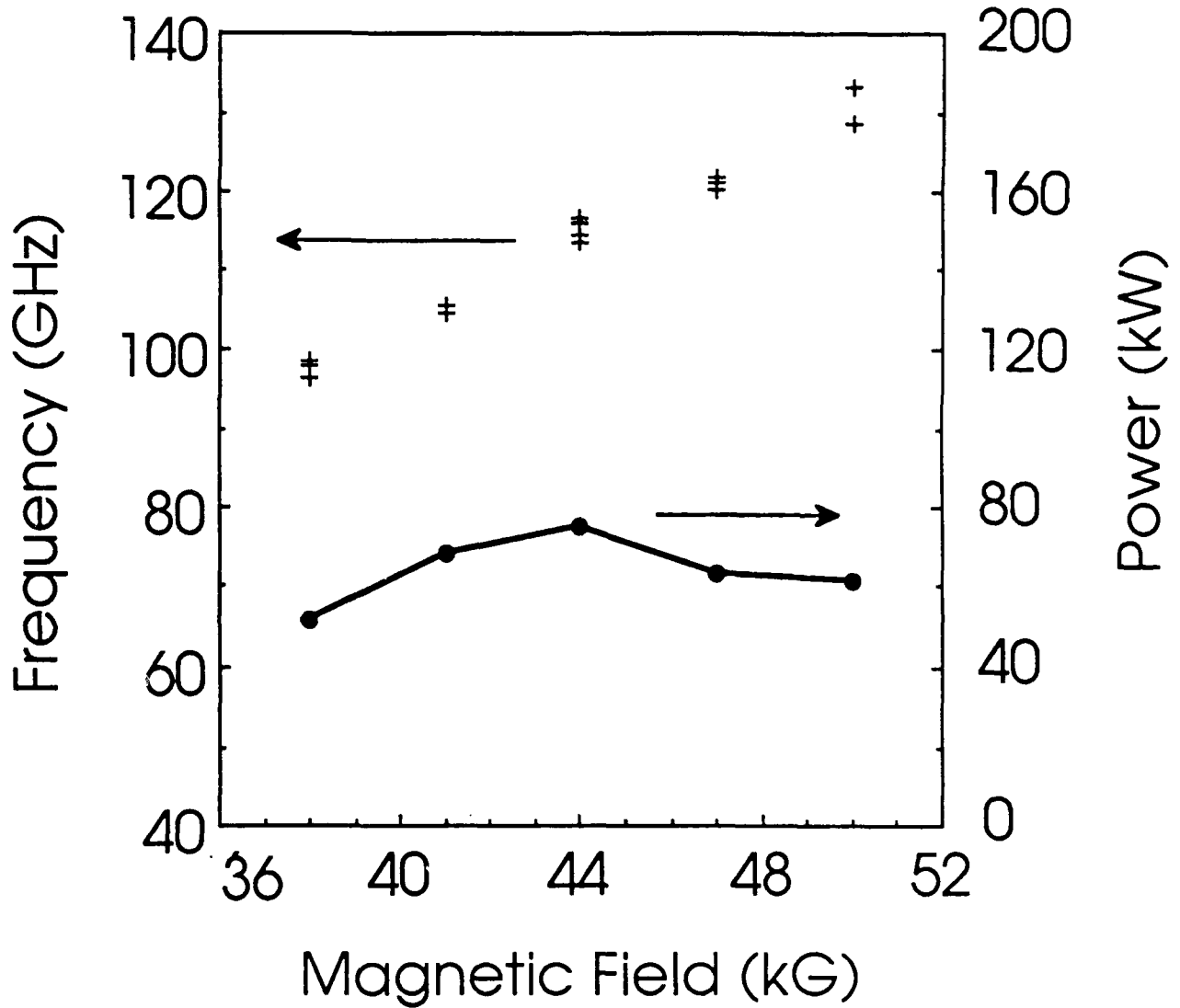


Fig. 4 — Tuning range of the quasi-optical gyrotron as a function of magnetic field

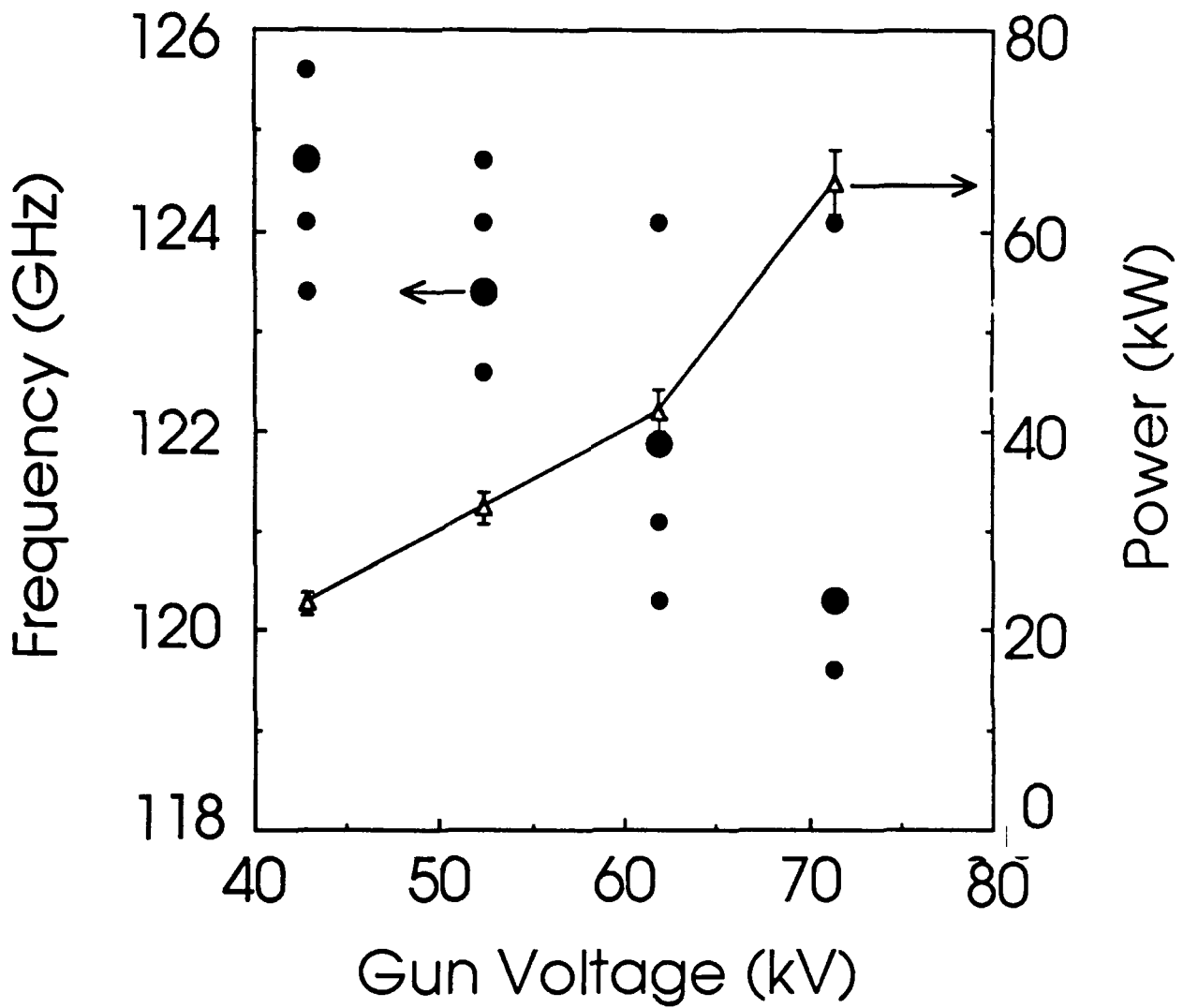


Fig. 5 — Tuning range of the quasi-optical gyrotron as a function of Voltage

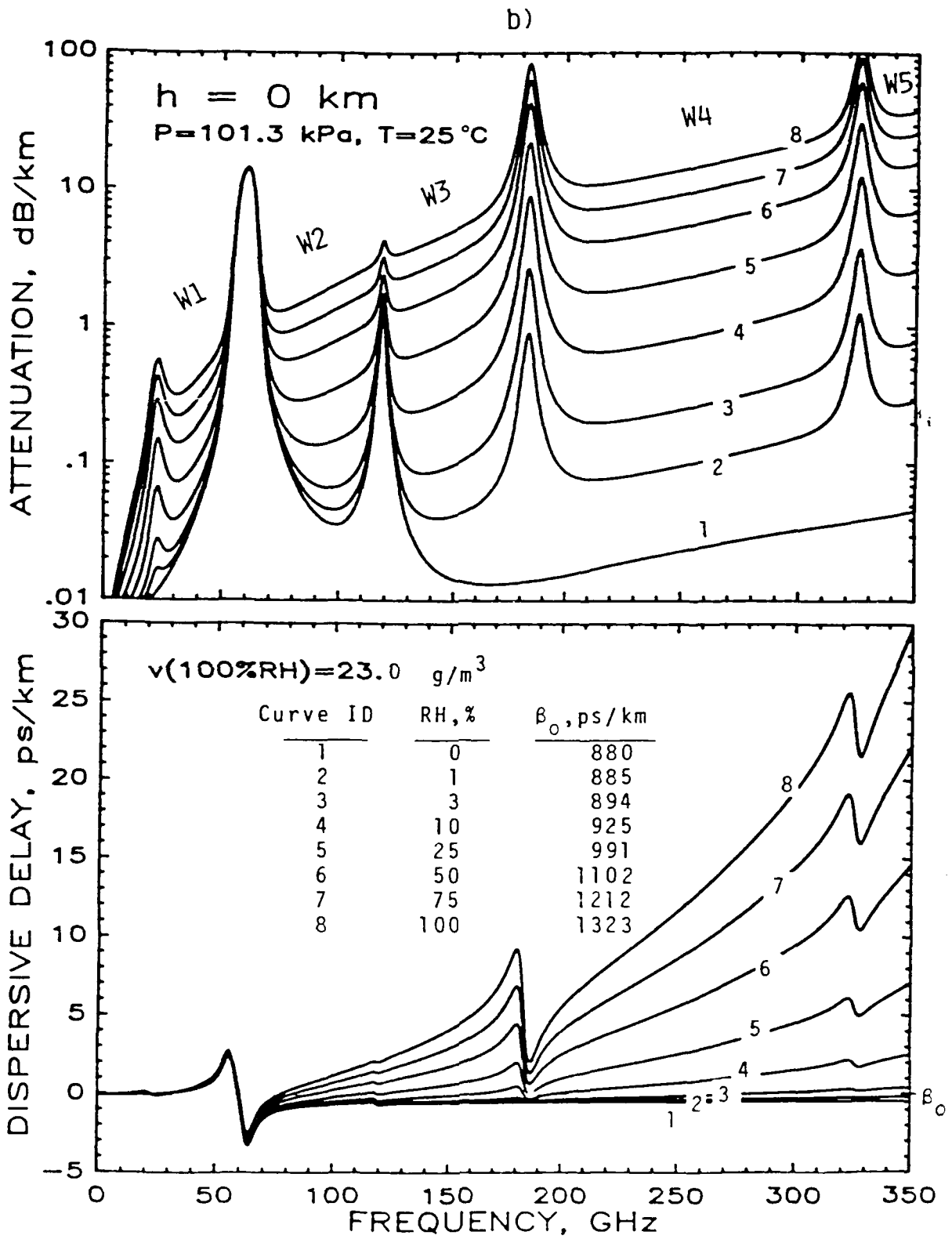


Fig. 6 — Attenuation (dB/km) and phase delay (ps/km) for atmospheric propagation as a function of frequency and humidity

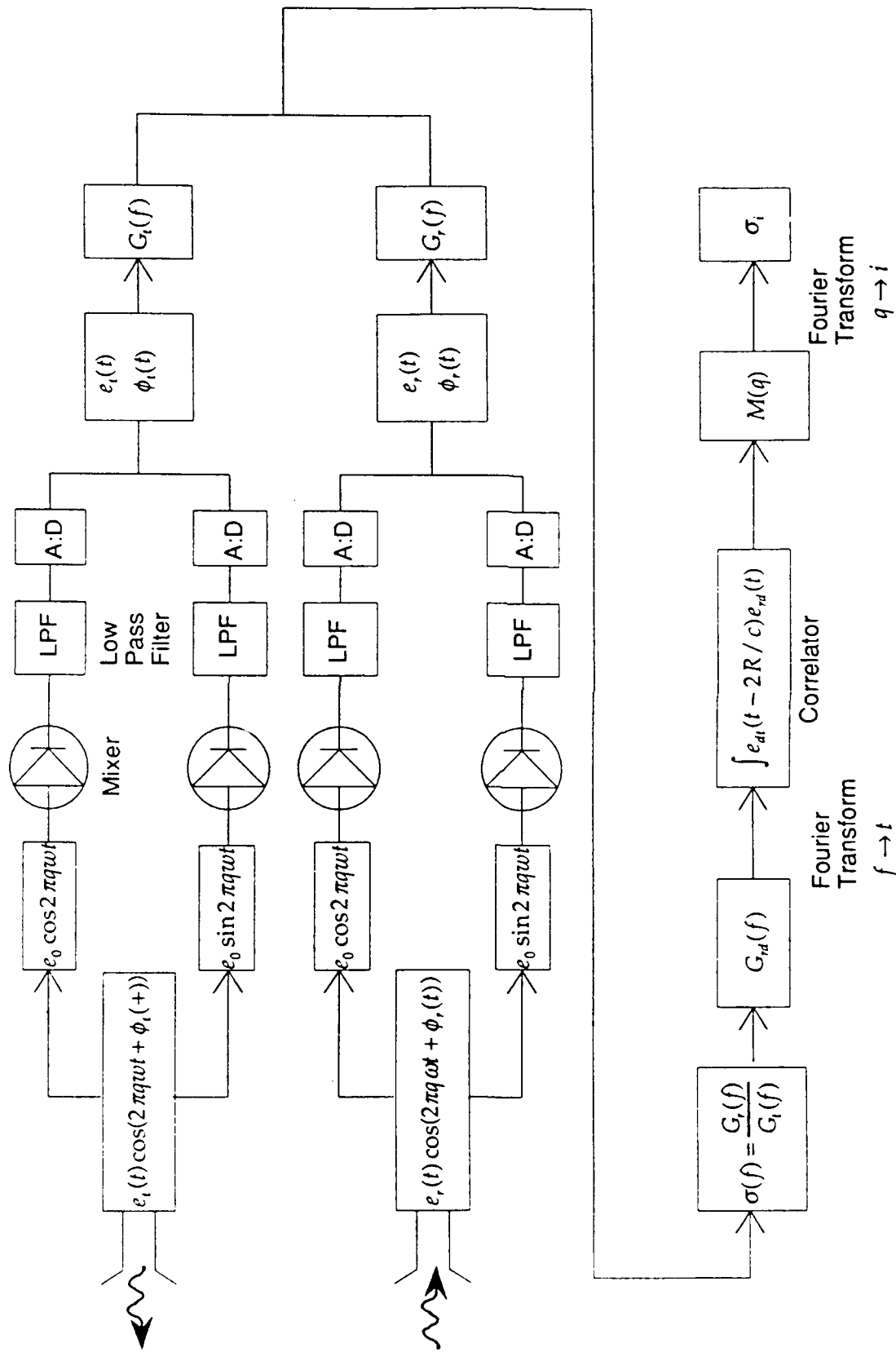


Fig. 7 — Circuit model for the quasi-optical gyrotrotron for super range resolution. After the A/D converter, the circuit elements are computer programs and the data are analyzed off line.

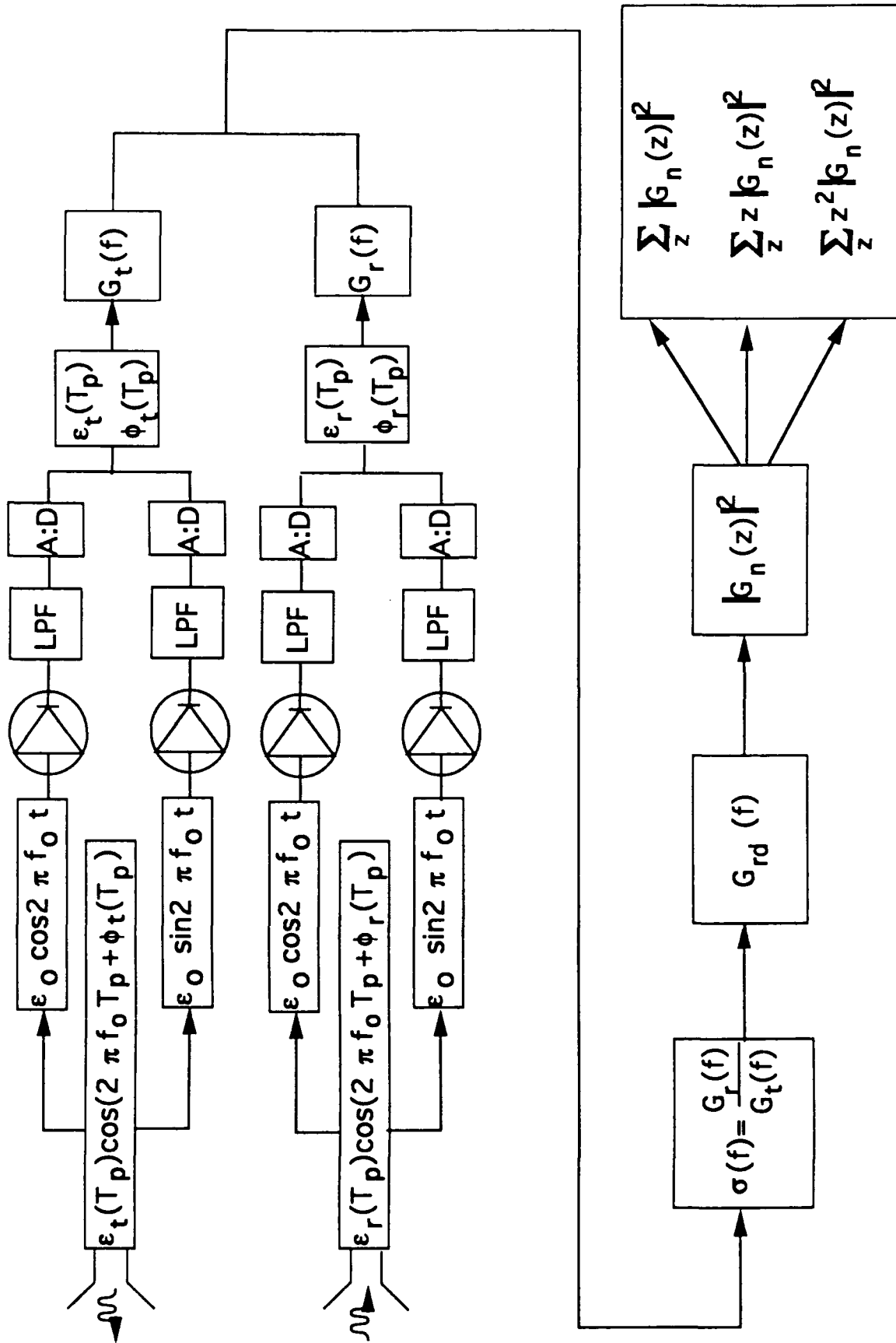


Fig. 8 — Circuit model for gyrotrotron based Doppler Cloud observation

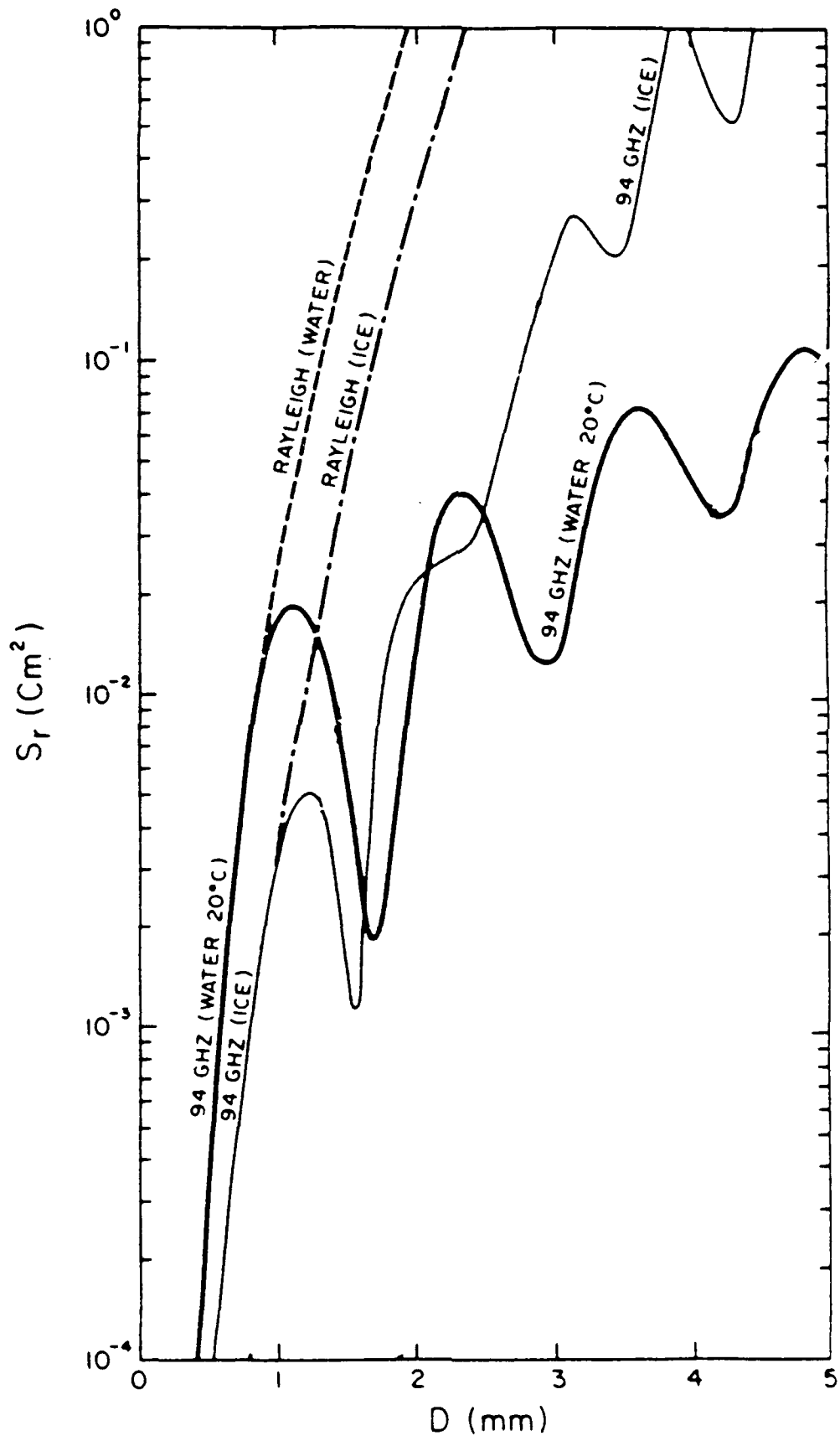


Fig. 9 — Mie scatter cross section for ice and water at 94 GHz.